Available online at www.sciencedirect.com
SCIENCE DIRECT
Precambrian Research 148 (2006) 225–256
Precambrian Research
www.elsevier.com/locate/precamres

Isotopic and geochemical evidence of proterozoic episodic crustal reworking within the irumide belt of south-central Africa, the southern metacratonic boundary of an Archaean Bangweulu Craton

Bert De Waele [a,*], Jean-Paul Liégeois [b], Alexander A. Nemchin [c], Francis Tembo [d]

[a] *Tectonics SRC, University of Western Australia, School of Earth and Geographical Sciences, 35 Stirling Highway, Crawley, WA 6009, Australia*
[b] *Isotope Geology Section, Africa Museum, B-3080 Tervuren, Belgium*
[c] *Tectonics SRC, Curtin University of Technology, Bentley, WA 6845, Australia*
[d] *Geology Department, School of Mines, University of Zambia, P.O. Box 32379, Lusaka, Zambia*

Received 19 January 2006; received in revised form 28 April 2006; accepted 12 May 2006

Abstract

Whole-rock geochemistry and Sr–Nd isotopic data for granitoids and volcanic rocks of four main different igneous phases, the Usagaran phase (2.05–1.93 Ga), the Ubendian phase (1.88–1.85 Ga), the Lukamfwa phase (1.65–1.55 Ga) and the Irumide phase (1.05–0.95 Ga), recognised along the southern margin of the Congo Craton in the Bangweulu Block and Irumide Belt of Zambia, demonstrate a long history of crustal recycling of a cryptic Archaean basement complex. The isotopic record indicates that a largely similar crustal source can be assigned to all these magmatic phases, with subtle differences in isotopic and geochemical record reflecting varying distance to orogenic activity during each of these episodes, and varying, but always minor amounts of juvenile mantle input. T_{DM} model ages, ranging between 3.3 and 2.8 Ga for the granitoids, and between 2.9 and 2.4 Ga for volcanic rocks, indicate preponderant Archaean crust within the Bangweulu Block and within the Irumide Belt. The corresponding initial ε_{Nd} values vary between −6 and −15 for the granitoids, and between −2 and −7 for the felsic volcanic rocks. Only some of the ca. 1.85 Ga mafic volcanic units record a more juvenile character ($\varepsilon_{Nd}(T)$ between −5 and 0 and T_{DM} model ages between 3.2 and 2.4 Ga) but still with a significant old crust input.

The geochemistry (major and trace elements) of the various magmatic groups shares many similarities indicating essentially similar crustal sources and conditions of melting. Only the anorogenic, 1.6 Ga, more alkaline granitoids, were generated through a lower degree of partial melting, but still from the same source.

Combining all available constraints, we propose that the Irumide Belt corresponds to the recurrently destabilised (at 2, 1.85, 1.6 and 1 Ga) southern boundary of the Bangweulu Block, whose preserved nucleus appears to be an Archaean craton covered by Palaeoproterozoic sediments. There are no juvenile subduction-related rocks in the Irumide Belt s.s., but such rocks are reported to the south, across the Mwembeshi Dislocation Zone (MDZ), in a region referred to as the Southern Irumide Belt.

Processes of endo-destabilisation in response to external forces (orogenies acting close or elsewhere), such as that recorded in the Bangweulu Block and the Irumide Belt s.s., correspond to a metacratonic evolution. Within the Irumide Belt itself, tectonic movements were mainly vertical, with horizontal movements restricted mainly to the supracrustal sequences.

Keywords: Geochemistry; Granite; Nd model age; Crustal reworking; Bangweulu Block; Irumide Belt; Metacraton

* Corresponding author.
E-mail address: info@bdewaele.be (B. De Waele).

0301-9268/$ – see front matter © 2006 Elsevier B.V. All rights reserved.
doi:10.1016/j.precamres.2006.05.006

1. Introduction

The Bangweulu Block forms part of the central African Congo Craton and is located in between two Mesoproterozoic provinces, the Kibaran Belt to the northwest and north, and the Irumide Belt to the southeast (Fig. 1). The eastern boundary of the Bangweulu Block is defined by a Neoproterozoic mega shear zone within the Palaeoproterozoic Ubendian Belt, the Mugesse Shear Zone, which separates the Bangweulu Block from the Tanzania Craton to the northeast. The same mega shear zone also marks the northeastern termination of the Mesoproterozoic Irumide Belt. A possible extension of the Bangweulu Block to the southwest is obscured by Neoproterozoic sedimentary rocks of the "Golfe du Katanga", and by thrusted metasedimentary rocks of the Katanga Supergroup within the Neoproterozoic Lufilian Belt. The Mesoproterozoic Irumide Belt occurs along the southeastern margin of the Bangweulu Block, and contains basement and supracrustal units of similar age to those reported in the Bangweulu Block. To the southeast of the Irumide Belt, the Mesozoic–Cenozoic Luangwa and Lukusashi grabens are present, which contain sediments of the Karoo Supergroup. These grabens appear to have largely evolved along a Proterozoic mega-shear zone, the Mwembeshi Dislocation Zone (MDZ), which marks the southern limit of the Irumide Belt. Precambrian units to the southeast of these grabens and the MDZ, in eastern Zambia and in northwestern Mozambique, mainly comprise late Mesoproterozoic juvenile terranes which may or may not have a geological affinity to the Irumide Belt and are referred to as the Southern Irumide Belt (Johnson et al., 2005b).

In this study, we present detailed field and geochemical/isotopic data for all recognised igneous phases in the Irumide Belt and the southern Bangweulu Block. The data shed new light on the tectonic evolution of the Irumide Belt, and on the nature of the Bangweulu Block, and form the basis to postulate a tentative geotectonic scenario for the evolution of the region within a context of crustal recycling, corresponding to a metacratonic evolution along a passive margin.

2. Geological background

The Bangweulu Block and Irumide Belt have, for long, remained enigmatic geological provinces, whose role in the regional tectonic framework of stable cratons and orogenic belts have been the subject of debate for many years. The terms "Zambia Craton" (Kröner, 1977), "Zambia nucleus" (Clifford, 1970), "Luwama Craton" (Pretorius in Hunter, 1981) or "Bangweulu Block" (Drysdall et al., 1972) were applied to the presumed Archaean basement of northern Zambia, extending along the shores of Lake Tanganyika into the Democratic Republic of Congo (hereafter Congo) and Tanzania. The term Bangweulu Block is here used to denote the pre-Irumide and pre-Kibaran basement units and overlying Palaeoproterozoic supracrustal sequences, and is delineated by the Palaeoproterozoic Ubendian Belt, the Mesoproterozoic Kibaran and Irumide Belts, and the Neoproterozoic Lufilian Belt (Fig. 1).

The term "Irumide Belt" was introduced by Ackermann (1950) to denote the strongly folded and metamorphosed southeastern margin of the Bangweulu Block, and the belt was interpreted as a Mesoproterozoic bi-vergent collisional belt.

2.1. The Bangweulu Block

The Bangweulu Block was first described in detail by Andersen and Unrug (1984), who considered it to comprise a crystalline basement of schist belts, intruded by coeval granitoids and metavolcanic rocks, and unconformably overlain by a thick sequence of fluvial, aeolian and lacustrine sediments (Fig. 1).

The schist belts occur along several east–west oriented zones of ca. 10 km wide and over 100 km long in the northeastern and eastern parts of the block, and in places appear to merge without discernable break with similar high-grade lithologies within the Ubendian Belt, while in other locations they are terminated along important shear zones. Further south, away from the

Fig. 1. (a) Regional tectonic framework of central-southern Africa. AKC, Angola Kasai Craton; KB, Kibaran Belt; EAO, East African Orogen; TC, Tanzania Craton; Ub, Ubendian Belt; Us, Usagaran Belt; BB, Bangweulu Block; LA, Lufilian Belt; IB, Irumide Belt; LuB, Lurio Belt; ZM, Zambezi Belt; CK, Choma-Kalomo Block; ZC, Zimbabwe Craton; NW, Northwest Botswana Rift; DB, Damara Belt; MaB, Magondi Belt; LiB, Limpopo Belt; SS, Sinclair Sequence; KvC, Kaapvaal Craton; NB, Namaqua Belt; NaB, Natal Belt; SaB, Saldania Belt. (b) Regional geological map showing location of samples reported in Tables 2 and 3. Abbreviated placenames: i, Isoka; c, Chinsali; M, Mpika; s, Serenje; m, Mkushi; c, Chipata; abbreviated lithological units: MpG, Mporokoso Group; MtH, Mututa Hills; KsF, Kasama Formation; LGG, Luwalizi Granite Gneiss; MfG, Mafingi Group; M, Mafinga Hills; MrG, Manshya River Group; KnG, Kanona Group.

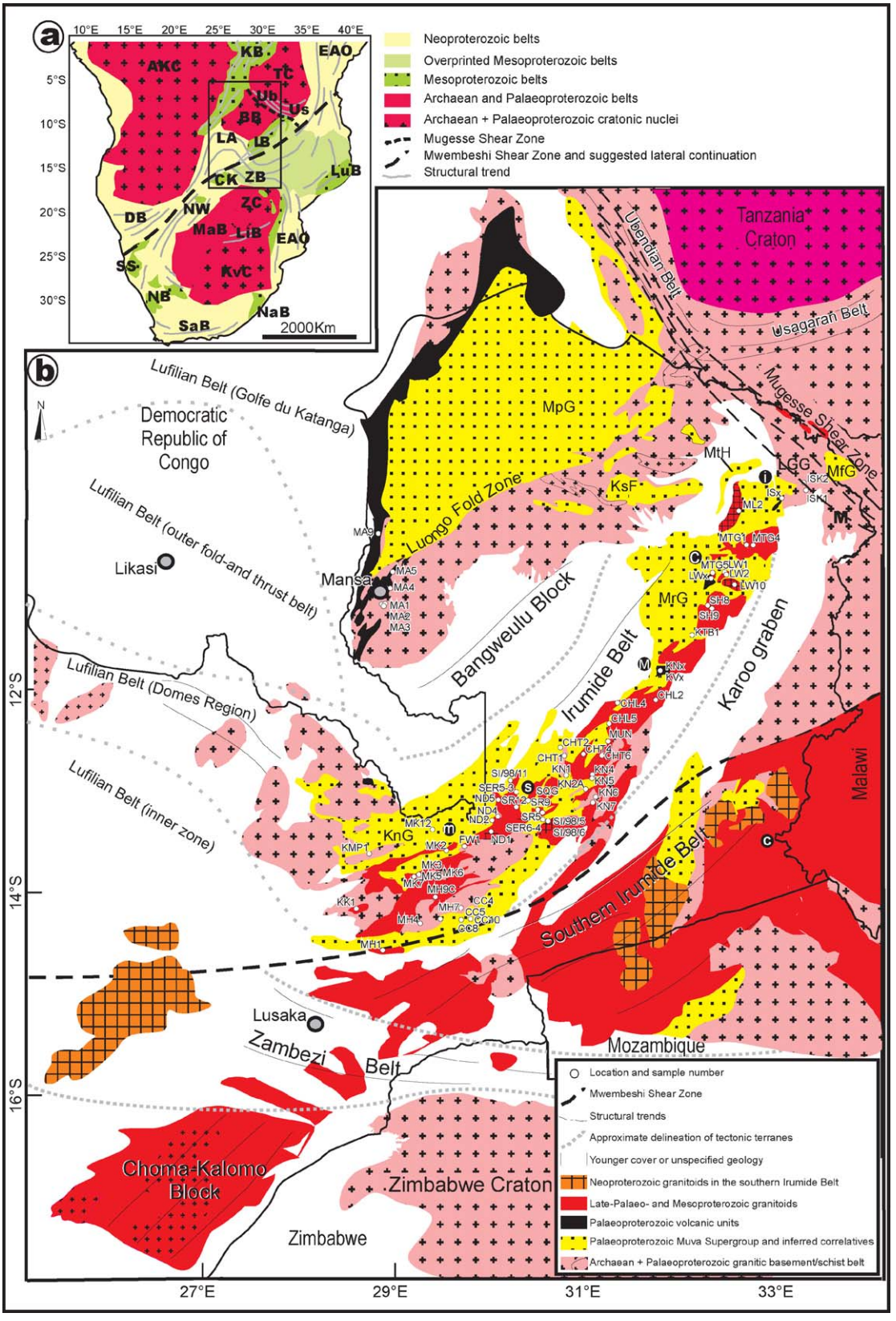
a
b
Neoproterozoic belts
Overprinted Mesoproterozoic belts
Mesoproterozoic belts
Archaean and Palaeoproterozoic belts
Archaean + Palaeoproterozoic cratonic nuclei
Mugesse Shear Zone
Mwembeshi Shear Zone and suggested lateral continuation
Structural trend
AKC
KB
TC
EAO
Ub
Us
BB
LA
LB
CK
ZB
LuB
ZC
NW
DB
MaB
LiB
EAO
SS
KvC
NB
NaB
SaB
2000Km
Tanzania Craton
Ubendian Belt
Usagaran Belt
Mugesse Shear Zone
Lufilian Belt (Golfe du Katanga)
Democratic Republic of Congo
Lufilian Belt (outer fold-and thrust belt)
Likasi
Mansa
Luongo Fold Zone
MpG
MtH
KsF
GG
MfG
Bangweulu Block
MrG
Irumide Belt
Karoo graben
Lufilian Belt (Domes Region)
Lufilian Belt (inner zone)
KnG
Malawi
Southern Irumide Belt
Lusaka
Zambezi Belt
Mozambique
Choma-Kalomo Block
Zimbabwe Craton
Zimbabwe
12°S
14°S
16°S
27°E
29°E
31°E
33°E
Location and sample number
Mwembeshi Shear Zone
Structural trends
Approximate delineation of tectonic terranes
Younger cover or unspecified geology
Neoproterozoic granitoids in the southern Irumide Belt
Late-Palaeo- and Mesoproterozoic granitoids
Palaeoproterozoic volcanic units
Palaeoproterozoic Muva Supergroup and inferred correlatives
Archaean + Palaeoproterozoic granitic basement/schist belt

Ubendian Belt, the schist belts are less extensive and form discrete septae or rafts within undeformed granitoids of the Bangweulu Block. The schist belts on the Bangweulu Block are dominated by strongly deformed chlorite, muscovite and biotite schist and recrystallised quartzite, but, towards the Ubendian Belt, the grade increases somewhat, with the appearance of migmatites and sillimanite and cordierite gneisses, while the structural trends swing from E–W into parallelism with Ubendian NNW–SSE trends. The Bangweulu granitoids comprise undeformed, coarse to porphyritic granites and granodiorites (Brewer et al., 1979; Schandelmeier, 1980, 1983). These plutons appear to represent shallow intrusions, as they were accompanied by andesitic to rhyolitic volcanism (Brewer et al., 1979). The volcanic units occur along the fringe of the supracrustal succession, and are reported to occur within the basal successions, indicating an overlap of deposition and volcanism. The volcanic units mainly comprise pyroclastic rocks (volcanic breccia, agglomerate and pyroclastic tuff), but also include minor hypabyssal intrusions and andesitic–rhyolitic flows. Both the granitoids and volcanic units display high-K calc-alkaline geochemistry and this led Andersen and Unrug (1984) to interpret them as a volcanic arc along an active plate-margin, postulated to lie to the northwest. Let us note however that there seems to be no evidence of significant crustal thickening and subsequent unroofing of the Bangweulu Block, which appears to consist largely of shallow level plutons and volcanic units.

The supracrustal sequences of the Bangweulu Block, late Palaeoproterozoic in age (ca. 1.8 Ga) include both undeformed units to the north, and strongly deformed and folded units within the Irumide Belt, and are collectively referred to as the Muva Supergroup (Daly and Unrug, 1982; De Waele and Fitzsimons, 2004; De Waele, 2005). The undeformed units on the Bangweulu Block comprise the Mporokoso Group, and a minor unit, the Kasama Formation, exposed in a discrete E–W oriented basin near Kasama (KsF, see Fig. 1). The Mporokoso Group is extensively described by Unrug (1984) and Andrews-Speed (1986, 1989), and comprises a 5-km-thick sequence of continental sediments, dominated by shallow water and lacustrine and minor aeolian units. Palaeocurrent analyses reported by Unrug (1984) indicate derivation from source terranes to the SE. The Kasama Formation consists of very mature clean quartz-arenites, in which palaeocurrent indicators show a derivation from the west. Unrug (1984) therefore considered the Kasama Formation to represent a second-cycle deposit derived from reworking of the Mporokoso Group.

2.2. The Irumide Belt

The Irumide Belt includes deformed basement units and metasedimentary successions, strongly metamorphosed to amphibolite facies, but also well-preserved Palaeoproterozoic volcanic sequences, the whole being intruded by voluminous high-K granitoids during the late-Mesoproterozoic Irumide orogeny (ca. 1.02 Ga). Recent reinterpretations of published geological reports and maps, and extensive zircon U–Pb Sensitive High mass Resolution Ion MicroProbe (SHRIMP) geochronology, have demonstrated that the Irumide Belt comprises a Palaeoproterozoic basement dated between 2.05 and 1.93 Ga (Rainaud et al., 2003, 2005; De Waele, 2005), intruded by a previously unrecognised magmatic suite called the Lukamfwa suite between 1.66 and 1.55 Ga (De Waele et al., 2003, in press; De Waele, 2005), and finally strongly deformed during the Irumide event at 1.02 Ga (De Waele et al., 2003, in press; De Waele, 2005). The Irumide event itself was accompanied by widespread high-K granite magmatism between 1.05 and 1.00 Ga with minor post-kinematic alkaline magmatism at ca. 0.95 Ga (De Waele, 2005). The deformed succession in the Irumide Belt comprises shallow marine quartzites and pelites, which have been termed the Kanona Group in the southwestern Irumide Belt and the Manshya River Group in the northeastern Irumide Belt (De Waele and Mapani, 2002). Dated volcanic units and detrital zircon age data indicate that these successions were deposited at least as early as 1.88 billion years ago, in a similar time-frame as the Mporokoso Group (De Waele, 2005).

2.3. The Southern Irumide Belt

To the south of the Mesozoic–Cenozoic Luangwa and Lukusashi Karoo grabens, located along the Proterozoic MDZ mega-shear zone, late Mesoproterozoic juvenile terranes are present. Preliminary whole-rock Sm–Nd and Rb–Sr data, and zircon Lu–Hf isotopic data seem to suggest that these granitoids are juvenile in character, with some contamination by crustal material (Johnson et al., 2005a). Magmatic emplacement ages ranging from 1.08 to 1.04 Ga have been documented for magmatic units, indicating that magmatism in the Southern Irumide Belt predated peak magmatic events in the Irumide Belt to the north (Johnson et al., 2005b).

3. Previous geochronology, geochemistry and isotopic data

The following sections provide a brief summary of published geochronological, isotopic or geochemical data for magmatic units in the Bangweulu Block and Irumide Belt. A short overview of available data is included on the Palaeoproterozoic Ubendian Belt, the evolution of which appears to be closely linked to the development of the Bangweulu Block. In this summary, we limit ourselves to dates which are perceived to be geologically meaningful, which include tightly constrained whole-rock Rb–Sr isochrons, mineral K–Ar or $^{40}Ar/^{39}Ar$ ages, zircon evaporation $^{207}Pb/^{206}Pb$ and zircon U–Pb (Thermal Ionisation Mass Spectrometry (TIMS) or SHRIMP) ages. These geochronological data are shown in Tables 1a and 1b, with locations in Fig. 2, and a summarised histogram with single zircon U–Pb SHRIMP ages reported in Table 1b from the Irumide Belt and Bangweulu Block in Zambia in Fig. 3.

3.1. The Ubendian Belt

Various deformed gneissic basement units within the southern Ubendian Belt have yielded zircon U–Pb and zircon $^{207}Pb/^{206}Pb$ evaporation ages of between 2093 ± 1 and 1932 ± 9 Ma (Dodson et al., 1975; Lenoir et al., 1994; Ring et al., 1997). These gneisses have subsequently been intruded by less- or undeformed granitoids, one of which yielded a zircon U–Pb TIMS age of 1864 ± 32 Ma (Lenoir et al., 1994), while several whole-rock Rb–Sr dates were reported adjacent to the Ubendian Belt between 1864 ± 32 and 1836 ± 86 Ma (Schandelmeier, 1983; Kabengele et al., 1991; Lenoir et al., 1994). Ring et al. (1997) considered a zircon $^{207}Pb/^{206}Pb$ age of 2002 ± 1 Ma and zircon $^{207}Pb/^{206}Pb$ ages ranging between 1995 ± 1 and 1988 ± 1 Ma on high-grade granite gneisses to reflect two distinct phases of peak granulite facies conditions, followed by intrusion of various granitoids between 1969 ± 1 and 1932 ± 9 Ma (Dodson et al., 1975; Ring et al., 1997). The geochemistry of these granitoids shows volcanic arc affinity, and Ring et al. (1997) interpreted the granitoid pulses between 2050 and 1930 Ma to reflect a long-lived Andean-type subduction zone. These ages are comparable to those found in the E–W oriented Usagaran Belt, adjacent to the east (Fig. 1). The Ubendian Belt was the locus of extensive shearing (e.g. Daly, 1988; Lenoir et al., 1994; Klerkx et al., 1998), possibly during the Palaeoproterozoic, but certainly during the late Mesoproterozoic, with the development of shear-controlled A-type granitoids dated between 1119 ± 20 and 1087 ± 11 Ma (Ring et al., 1999). Irumide orogenesis, characterised by extensive crustal shortening (Daly, 1986), is assumed to have utilised a lateral ramp system along the Mugesse Shear Zone, but this assumption awaits detailed geochronology on this mega shear. Neoproterozoic reactivation of the shear zones in the Ubendian Belt provoked the intrusion of alkaline granitoids and syenites between 743 ± 20 and 724 ± 6 Ma (Lenoir et al., 1994), while the region appears to have been reactivated several times since, to form part of the East African Rift system (Klerkx et al., 1998).

3.2. The Bangweulu Block

Various Rb–Sr dates have been reported for granitoids in the eastern part of the Bangweulu Block, adjacent to the Ubendian Belt, and range from 1869 ± 40 to 1824 ± 126 Ma (Schandelmeier, 1983). These ages are very similar to whole-rock Rb–Sr ages reported on granitoids and volcanics in the western part of the Bangweulu Block near Mansa by Brewer et al. (1979), 1833 ± 18 and 1812 ± 22 Ma, respectively, and a Rb–Sr age of 1861 ± 28 Ma reported to the north from the part of the Bangweulu Block to the west of Lake Tanganyika in Congo (Kabengele et al., 1991). Farther west, within the Domes Region of the Copperbelt, John (2001) reported zircon TIMS ages of 1874 ± 9 and 1884 ± 10 Ma for granitoids of the Solwezi and Kabompo Domes, respectively, while Ngoyi et al. (1991) and Rainaud et al. (2002) reported U–Pb zircon ages of 1882 ± 20 and 1873 ± 8 Ma for granitoids and metavolcanic rocks of the Luina Dome, respectively. These data seem to indicate the presence of an extensive plutono-volcanic province stretching from the Ubendian Belt to the east into the Domes Region of the Copperbelt to the west. Kabengele et al. (1991) as well as Brewer et al. (1979) interpreted these ca. 1.85 Ga plutono-volcanic rocks to represent a large volcanic-arc along an active convergent margin. Lenoir et al. (1994) used similarities in age between tectonothermal events in the Usagaran and Ubendian Belts to suggest a long-lasting active continental margin along the southern margin of the Tanzania and Congo Craton, terminated by transpressive shear along the Ubendian Belt and intrusion of the 1.8 Ga plutono-volcanic suite.

The youngest dated rocks in the Bangweulu Block are the Lusenga Syenite, which yielded a whole-rock Rb–Sr date of 1145 ± 20 Ma (Brewer et al., 1979), and various mafic dykes, which yielded poorly constrained K–Ar or $^{40}Ar/^{39}Ar$ ages of between 1040 and 700 Ma (Schandelmeier, 1983; Daly, 1986), but until more reli-

Table 1a
Previously published and unpublished Proterozoic age data (>ca. 950 Ma) for Zambia and northern Malawi (refer to Fig. 2 using grid squares for location)

Sample ID	Age ± error (Ma)	Grid square	Method	Source
Kaunga Granite	970 ± 5	C11	U–Pb TIMS bulk zircon	Daly (1986)
Aplite (Luromo Granite)	977 ± 1	C13	Pb evaporation single zircon	Ring et al. (1999)
Aplite (Wililo Granite)	983 ± 1	B12	Pb evaporation single zircon	Ring et al. (1997)
Porphyritic granite (ZAM5)	1041 ± 9	F11	U–Pb SHRIMP zircon	De Waele (2005)
Luangwa gneiss	*1043 ± 19*	G9	LA-ICP-MS	Cox et al. (2002)
Chipata granulite	1046 ± 3	F11	U–Pb TIMS single monazite	Schenk and Appel (2001)
Madzimoyo Gneiss (ZAM1)	*1047 ± 20*	F11	U–Pb SHRIMP zircon	De Waele (2005)
Porphyritic granite (ZAM4)	1050 ± 10	F11	U–Pb SHRIMP zircon	De Waele (2005)
Porphyritic granite (ZAM3)	1074 ± 3	F11	U–Pb SHRIMP zircon	De Waele (2005)
Phoenix Mine mica	1080 ± 31	16	Rb–Sr mica	Cahen et al. (1984)
Lwakwa Granite	1087 ± 11	B12	U–Pb TIMS single zircon	Ring et al. (1999)
Mkushi Gneiss	1088 ± 159	F8	U–Pb SHRIMP zircon	Rainaud et al. (2002)
Munali Granite	1090 ± 1	H8	U–Pb TIMS single zircons	Katongo et al. (2004)
Mpande Gneiss	1106 ± 19	H7	U–Pb TIMS bulk zircon	Hanson et al. (1988a)
Luromo Granite	1108 ± 1	C13	Pb evaporation single zircon	Ring et al. (1999)
Wililo Granite	1115 ± 1	B12	Pb evaporation single zircon	Ring et al. (1999)
Wililo Granite	1116 ± 1	B12	Pb evaporation single zircon	Ring et al. (1999)
Wililo Granite	1118 ± 1	B12	Pb evaporation single zircon	Ring et al. (1999)
Mwenga Granite	1119 ± 20	B12	U–Pb TIMS single zircon	Ring et al. (1999)
Lusenga Syenite	1134 ± 8	A8	Whole-rock Rb–Sr	Brewer et al. (1979)
Granite (Choma-Kalomo block)	1174 ± 27	J5	U–Pb SHRIMP zircon	Bulambo et al. (2004)
Granite (Choma-Kalomo block)	1177 ± 70	I6	U–Pb SHRIMP zircon	Bulambo et al. (2004)
Granite (Choma-Kalomo block)	1181 ± 9	I6	U–Pb SHRIMP zircon	Bulambo et al. (2004)
Granite (Choma-Kalomo block)	1188 ± 11	J5	U–Pb SHRIMP zircon	Bulambo et al. (2004)
Semahwa Gneiss	1198 ± 6	I6	U–Pb TIMS bulk zircon	Hanson et al. (1988b)
Siasikabole Granite	1232 ± 20	J6	Whole-rock Rb–Sr	Hanson et al. (1988b)
Chilala Gneiss	1285 ± 64	I6	U–Pb TIMS bulk zircon	Hanson et al. (1988b)
Ntendele metatonalite	1329 ± 1	C12	Pb evaporation single zircon	Vrána et al. (2004)
Mivula Syenite	1341 ± 16	C12	Whole-rock Rb–Sr	Tembo (1986)
Zongwe Gneiss	1343 ± 6	J6	U–Pb TIMS bulk zircon	Hanson et al. (1988b)
Siasikabole Granite	1352 ± 14	J6	U–Pb TIMS bulk zircon	Hanson et al. (1988b)
Mivula Syenite	1360 ± 1	C12	Pb evaporation single zircon	Vrána et al. (2004)
Granite (Choma-Kalomo block)	1368 ± 10	J6	U–Pb SHRIMP zircon	Bulambo et al. (2004)
Mutangoshi Gneissic Granite	1407 ± 33	C11	Whole-rock Rb–Sr	Daly (1986)
Mwambwa River Gneiss	1804 ± 170	C11	Whole-rock Rb–Sr	Daly (1986)
Luchewe Granite	1830 ± 240	B11	Whole-rock Rb–Sr	Schandelmeier (1980)
Mansa Volcanic	1815 ± 29	D8	Whole-rock Rb–Sr	Brewer et al. (1979)
Mansa Granite	1832 ± 32	D8	Whole-rock Rb–Sr	Brewer et al. (1979)
Kate Granite	1839 ± 80	A10	Whole-rock Rb–Sr	Schandelmeier (1980)
Kinsenda Lufubu Schist	1873 ± 8	E7	U–Pb SHRIMP zircon	Rainaud et al. (2002)
Solwezi Granite	1874 ± 9	E4	U–Pb TIMS single zircon	John (2001)
Mambwe Gneiss	1870 ± 39	B10	Whole-rock Rb–Sr	Schandelmeier (1980)
Kinsenda Granite (Luina dome)	1882 ± 23	E7	U–Pb TIMS single zircon	Ngoyi et al. (1991)
Kabompo Granite	1884 ± 10	D4	U–Pb TIMS single zircon	John (2001)
Nyika Granite	1932 ± 9	C12	U–Pb TIMS bulk zircon	Dodson et al. (1975)
Kabompo Dome granite	1934 ± 6	D4	U–Pb zircon	Key et al. (2001)
Kabompo Dome granite	1940 ± 3	D4	U–Pb zircon	Key et al. (2001)
Biotite metatonalite	1961 ± 1	C12	Pb evaporation single zircon	Vrána et al. (2004)
Samba porphyry	1964 ± 12	E6	U–Pb SHRIMP zircon	Rainaud et al. (2002)
Nyika Granite	1969 ± 1	C12	Pb evaporation single zircon	Ring et al. (1997)
Lufubu Schist	1970 ± 10	E7	U–Pb SHRIMP zircon	Rainaud et al. (2002)
Mafic enclave in Gneiss (ZAM2)	1974 ± 18	F11	U–Pb SHRIMP zircon	De Waele (2005)
Mulungushi Gneiss	1976 ± 5	G7	U–Pb SHRIMP zircon	Rainaud et al. (2002)
Chambishi Granite	1980 ± 7	E7	U–Pb SHRIMP zircon	Rainaud et al. (2002)
Chambishi Granite	1983 ± 5	E7	U–Pb SHRIMP zircon	Rainaud et al. (2002)
Rumphi Granite	1988 ± 1	C13	Pb evaporation single zircon	Ring et al. (1997)
Mufulira Granite	1991 ± 3	E7	U–Pb SHRIMP zircon	Rainaud et al. (2002)

Table 1a (*Continued*)

Sample ID	Age ± error (Ma)	Grid square	Method	Source
Chelinda Granite	1995 ± 1	C12	Pb evaporation single zircon	Ring et al. (1997)
Luromo Granite	2002 ± 1	C13	Pb evaporation single zircon	Ring et al. (1997)
Luangwa gneiss	∼2033	G9	LA-ICP-MS	Cox et al. (2002)
Rumphi Granite	2048 ± 1	D13	Pb evaporation single zircon	Ring et al. (1997)
Mkushi Gneiss	2049 ± 6	F8	U–Pb SHRIMP zircon	Rainaud et al. (2002)
Mwinilunga granite	2058 ± 7	D3	U–Pb SHRIMP zircon	Key et al. (2001)
Luromo Granite	2093 ± 1	C13	Pb evaporation single zircon	Ring et al. (1997)
Luromo Granite	2224 ± 1	C13	Pb evaporation single zircon	Ring et al. (1997)
Mufulira quartzite	Detrital	E7	U–Pb SHRIMP zircon	Rainaud et al. (2002)

Italics date the growth of metamorphic zircon.

able age data become available on those units, not much weight is given to these particular age determinations.

It can be concluded that most of the known ages in the Bangweulu Block are in the 1.9–1.8 Ga range but we note that they are confined to its rims, its central part being covered by subhorizontal Palaeoproterozoic sediments.

3.3. The Irumide Belt

For long, the timing of magmatic and metamorphic events in the Irumide Belt had remained poorly constrained on the basis of few and imprecise Rb–Sr and bulk zircon U–Pb ages. Daly (1986), who concentrated on the northeastern Irumide Belt, reported a whole-rock Rb–Sr date of 1407 ± 33 Ma for the strongly deformed Mutangoshi Granite Gneiss to reflect an earlier magmatic episode during crustal extension, and the strongly disturbed Rb–Sr systematics for the Mwambwa Gneiss, with a subset of data regressing to a date of ca. 1100 Ma, to reflect peak metamorphism. A bulk zircon U–Pb age of 970 Ma for the Kaunga Granite, an undeformed pluton in the northeastern Irumide Belt, was interpreted to record post-kinematic magmatism after the Irumide orogeny. More recently, these ages have been drastically revised by work in the southwestern and northeastern Irumide Belt, revealing a Palaeoproterozoic basement complex, comprising orthogneisses aged between 2050 ± 9 and 1952 ± 6 Ma in the southwest (De Waele and Mapani, 2002; Rainaud et al., 2002, 2003; De Waele, 2005), and between 1961 ± 1 and 1927 ± 10 Ma in the northeastern Irumide Belt (Vrána et al., 2004; De Waele, 2005). In the far southwestern part of the Irumide Belt, one granitic gneiss yielded a zircon U–Pb SHRIMP age of 2726 ± 36 Ma (De Waele, 2005), directly confirming the presence, although limited, of an Archaean component within the belt. A second magmatic pulse is recognised both in the southwestern and northeastern Irumide Belt, with zircon U–Pb SHRIMP ages between 1664–1627 and 1610–1551 Ma, respectively (De Waele et al., 2003; De Waele, 2005). A previously reported anorogenic magmatic suite, with zircon $^{207}Pb/^{206}Pb$ ages between 1360 ± 1 and 1329 ± 1 Ma, identified to the east of the Luangwa graben in the northeastern part of the belt (Tembo, 1986; Vrána et al., 2004), has so far not been recognised in the Irumide Belt itself. Peak Irumide metamorphism is constrained by U–Pb SHRIMP ages on low Th/U zircon rims in high-grade migmatites in the southwestern Irumide Belt at ca. 1020 Ma, and by similar low Th/U zircon rims within metagranite in the northeastern Irumide Belt (De Waele, 2005). Irumide tectonism was accompanied by voluminous magmatism producing K-feldspar porphyritic granitoids and coarse biotite granitoids of predominant granitic and granodioritic composition. An extensive dataset of zircon U–Pb SHRIMP crystallisation ages indicates that this magmatism spanned between 1050 and 1000 Ma with minor post-kinematic granitoids between 970 ± 5 and 943 ± 5 Ma (Daly, 1986; De Waele and Mapani, 2002; De Waele, 2005). The youngest dated intrusions in the Irumide Belt comprise minor mafic dykes (amphibolites) which yielded $^{40}Ar/^{39}Ar$ ages between ca. 1040 and 935 Ma (Daly, 1986), and were interpreted to date uplift and cooling during and after the Irumide event.

Tembo et al. (2002) reported a limited geochemical dataset (major and trace element geochemistry) on granitoids in the Irumide Belt, and concluded that all granitic suites share broadly similar major and trace element patterns, with crust-dominated characteristics indicating that the petrogenetic processes responsible for their intrusion stayed remarkably uniform through the various tectonic stages shaping the belt. Trace element patterns, showing negative anomalies for Nb, Ti, P and Sr, and high HFSE contents, suggest a significant crustal input in the generation of all magmas, which was inferred to be an underlying Palaeoproterozoic magmatic arc.

Table 1b
Zircon U–Pb SHRIMP data for the Irumide Belt and Bangweulu Block (De Waele, 2005)

ID*	Sample	Rock type	Age (Ma)	*N*	C (%)	Age type
1	SER6-7	Fukwe Migmatite	*554 ± 20*	1	90	$^{207}Pb/^{206}Pb$
2	LW2	Luswa Syenite	943 ± 5	3	98–100	Concordia age
3	ZM32	Chilubanama Granite	~946 ± 50	1	106	$^{207}Pb/^{206}Pb$
4	SH8	Lufila Granite	1001 ± 44	2	80–94	W.M. $^{207}Pb/^{206}Pb$
5	KK1	Porphyritic granite	1003 ± 31	5	94–104	W.M. $^{207}Pb/^{206}Pb$
6	MTG4	Chilubanama Granite	*1004 ± 16*	4	98–101	Concordia age
7	LW1	Chilubanama Granite	1005 ± 21	1	100	$^{207}Pb/^{206}Pb$
8	CHT6	Biotite granite gneiss	1005 ± 7	9	92–127	Concordia age
9	MTG4	Chilubanama Granite	1010 ± 22	3	98–107	Concordia age
10	SASA2	Sasa Granite	1016 ± 14	6	95–103	Concordia age
11	CHL5	Granite gneiss	1016 ± 17	6	96–103	Concordia age
12	MH4	Porphyritic granite	1017 ± 19	2	99–102	Concordia age
13	SER6-6	Lukusashi migmatite	*1018 ± 5*	10	95–101	W.M. $^{207}Pb/^{206}Pb$
14	SER6-7	Fukwe Migmatite	*1021 ± 16*	8	93–98	W.M. $^{207}Pb/^{206}Pb$
15	KN8	Biotite granite gneiss	1022 ± 16	9	76–100	Upper intercept
16	ND1	Porphyritic granite	1023 ± 7	5	99–103	W.M. $^{207}Pb/^{206}Pb$
17	SQG	Serenje Quarry Granite	1024 ± 9	6	96–103	W.M. $^{207}Pb/^{206}Pb$
18	ZM36	Mununga Quarry Granite	1025 ± 10	10	84–108	Concordia age
19	ND5	Syeno-granite	1028 ± 7	2	100–102	Concordia age
20	MH9C	Porphyritic granite	1029 ± 14	7	95–102	W.M. $^{207}Pb/^{206}Pb$
21	MTGG1	Mutangoshi Gneissic Granite	1029 ± 9	8	91–102	Upper intercept
22	KN2A	Porphyritic granite	1031 ± 14	8	76–100	Upper intercept
23	ND4	Granodiorite	1031 ± 5	4	97–101	Concordia age
24	SER5-3	Porphyritic granite	1034 ± 5	7	98–105	Concordia age
25	MK7	Porphyritic granite	~1035 ± 32	1	94	$^{207}Pb/^{206}Pb$
26	CC8	Porphyritic granite	1035 ± 12	5	97–100	Concordia age
27	SER6-4	Porphyritic granite	1036 ± 13	8	85–103	Upper intercept
28	CC5	Porphyritic granite	1038 ± 17	6	94–105	Concordia age
29	FW1	Porphyritic granite	1038 ± 58	4	99–103	Upper intercept
30	KN7	Porphyritic granite	1048 ± 10	1	100	$^{207}Pb/^{206}Pb$
31	KN5	Biotite granite gneiss	1053 ± 14	8	87–100	Upper intercept
32	MTGG-2	Mutangoshi Gneissic Granite	1055 ± 13	3	101–106	Concordia age
33	ML2	Lubu Granite Gneiss	1551 ± 33	9	83–99	Upper intercept
34	LW10	Musalango Gneiss	1610 ± 26	8	93–101	W.M. $^{207}Pb/^{206}Pb$
35	ND2	Granite gneiss	1627 ± 12	4	98–102	Concordia age
36	SR12	Lukamfwa Hill Granite Gneiss	1639 ± 14	7	98–101	W.M. $^{207}Pb/^{206}Pb$
37	SER6-3	Lukamfwa Hill Granite Gneiss	1652 ± 6	10	97–102	Concordia age
38	SER6-2C	Lukamfwa Hill Granite Gneiss	1664 ± 6	8	98–104	Concordia age
39	IS20	Kachinga Tuff	1856 ± 4	7	98–101	Concordia age
40	MA1	Mansa Granite	1860 ± 13	4	90–99	Upper intercept
41	MA5	Mansa Volcanic	1862 ± 19	4	90–102	Upper intercept
42	MA2	Mansa granite	1862 ± 8	9	98–103	Concordia age
43	MA9	Musonda Falls Granite	1866 ± 9	6	99–102	Concordia age
44	MA3	Mansa Volcanic	1868 ± 7	8	98–103	Concordia age
45	KB5	Katibunga Basalt	1871 ± 24	6	93–99	W.M. $^{207}Pb/^{206}Pb$
46	ZM31	Luswa River Tuff	1879 ± 13	10	95–103	Concordia age
47	ISK2	Luwalizi Granite Gneiss	1927 ± 10	4	97–102	W.M. $^{207}Pb/^{206}Pb$
48	ISK1	Luwalizi Granite Gneiss	1942 ± 6	7	93–99	W.M. $^{207}Pb/^{206}Pb$
49	CC10	Porphyritic granite gneiss	1952 ± 6	5	95–104	Concordia age
50	MK5	Mkushi Gneiss	2029 ± 7	2	87–98	W.M. $^{207}Pb/^{206}Pb$
51	KN1	Mkushi Gneiss	2036 ± 6	5	93–100	W.M. $^{207}Pb/^{206}Pb$
52	MK3	Mkushi Gneiss	2042 ± 10	3	90–98	W.M. $^{207}Pb/^{206}Pb$
53	MK5	Mkushi Gneiss	2050 ± 9	4	95–100	W.M. $^{207}Pb/^{206}Pb$
54	KMP1	Kapiri Mposhi Granite	2726 ± 36	5	80–101	Upper intercept

Refer to Fig. 2 using ID* for location. Italics date the growth of metamorphic zircon. *N*: number of analysis points used to obtain the age. C (%) = (100 − ($^{207}Pb/^{206}Pb$ age))/(($^{206}Pb/^{238}U$ age) − 1). Age type refers to specific calculation method used to obtain an age for the sample set.

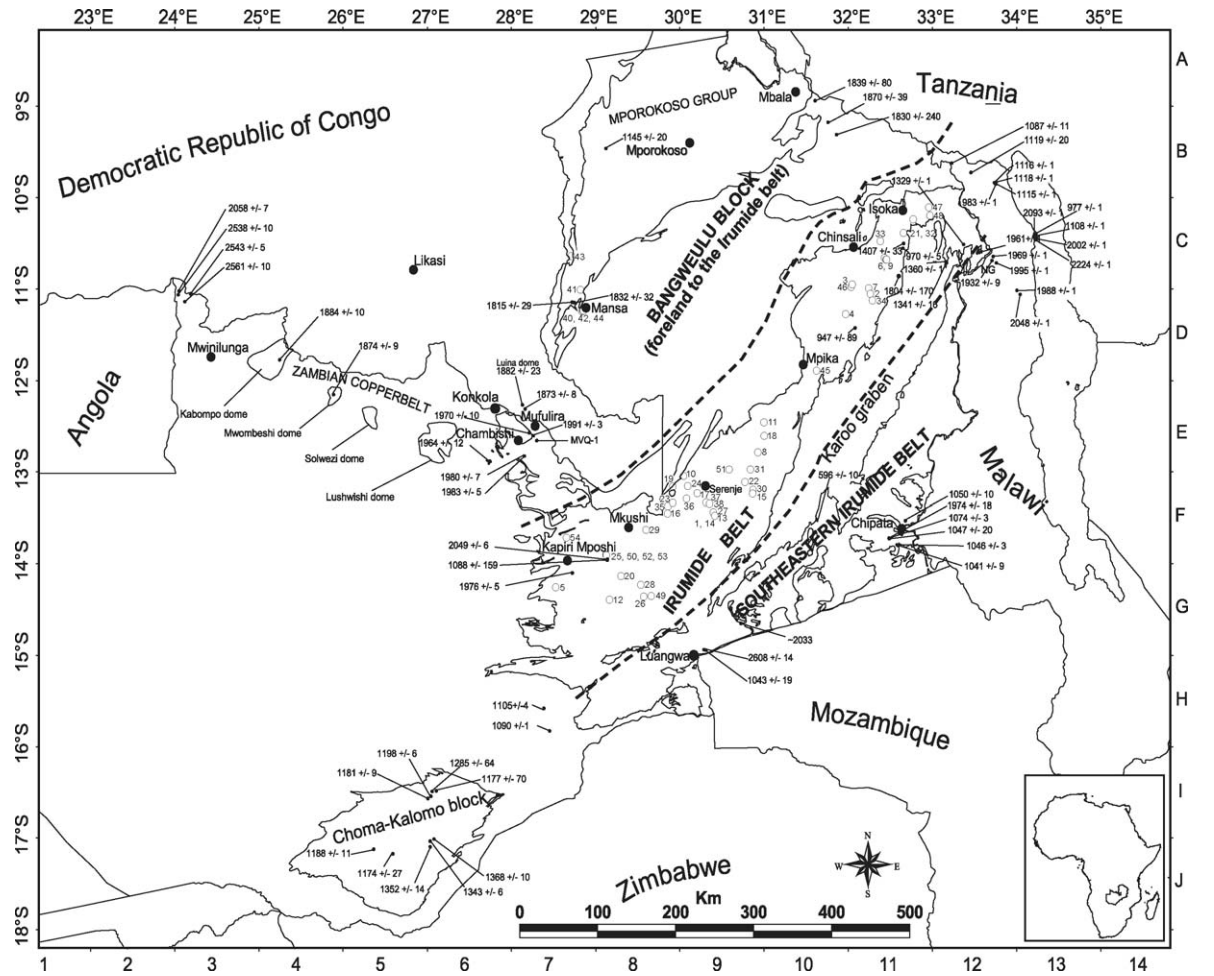

Fig. 2. Map showing the location of dated samples discussed in text and reported in Tables 1a and 1b. The outlines of international borders, the Mporokoso Group sedimentary succession, the Irumide Belt and Choma-Kalomo Block are shown for orientation purposes. Samples reported in Table 1a are labelled with the age, while samples reported in Table 1b are labelled with an identification number.

4. Methodology

4.1. Geochemistry

Samples were analysed in part by commercial laboratories (see Table 2), but a significant number were analysed by the first author at the analytical facilities of the Department of Applied Chemistry, Curtin University of Technology, Perth, Australia. The methodologies followed were broadly similar and are described below. Fresh rock samples were crushed using jaw-crusher, and pulverised using a tungsten-carbide ring-mill and two ~50 mg sample aliquots taken from the powder. One aliquot was digested using a mixed HF and $HNO_3/HClO_4$ digestion technique similar to that reported by Crock and Lichte (1982). Total digestion was checked visually, and the digestion process repeated as necessary. The digested samples were measured on the VG PQ3 ICP-MS instrument at the Department of Applied Chemistry at Curtin University of Technology. Standards were introduced with concentrations of 1, 2, 5, 10 and 20 ppb, while an internal Rh and Ir standard was applied for drift correction. The second aliquot was mixed with lithium tetraborate and fused in a platinum crucible at 970 °C. The fusion bead was dissolved in diluted HCl solution, which was analysed on the JY38 Sequential ICP-OES setup at the Department of Applied Chemistry at Curtin University of Technology. Natural rock standards and blank solutions were analysed as part of the sample sets, and together with duplicate analyses, allowed internal checks of the data quality. Cross-laboratory checks were also conducted to ensure reproducibility of the analyses.

Table 2
Whole-rock chemistry for magmatic rocks in northern Zambia

	ID															
	KMP1	*MK12*	*KN1*	*MK3*	*MK5*	*ISK1*	*ISK2*	*KN6*	*CC10*	*MA1*	*MA2*	*MA9*	*MA3*	*MA4*	*KV4*	*KB3*
Type	G_0	G_0	G_{1a}	G_{1a}	G_{1a}	G_{1b}	G_{1b}	G_{1b}	G_{1b}	G_{1c}, Gr	G_{1c}, Gr	G_{1c}, Gr	G_{1c}, dac	G_{1c}, dac	G_{1c}, bas	G_{1c}, bas
Age[a] (Ma)	2730		2036	2042	2029	1942	1927		1952	1860	1862	1866	1868			
SiO_2	71.8	70.1	69.2	70.8	75.5	67.8	73.6	73.9	74		72	78	68.6	66	47.4	48
TiO_2	0.37	0.37	0.67	0.66	0.28	1.24	0.43	0.14	0.33		0.6	0.17	0.68	0.73	2	0.83
Al_2O_3	15.5	17.4	14.6	15.5	12.5	13.8	13.5	14.2	13.8		13.3	12.2	16.2	16.2	13.4	18.3
Fe_2O_3	2.4	1.82	3.76	4.05	1.49	5.97	2.31	1.02	2.31		3.84	0.85	2.98	3.57	16.2	8.68
MnO															0.23	0.13
MgO	0.76	0.61	1.22	0.61	0.5	1.61	0.76	0.2	0.43		0.92	0.23	0.99	1.2	6.45	5.36
CaO	2.2	1.31	3.76	1.66	0.82	2.54	0.81	0.77	1.51		2.04	0.55	2.58	4.52	10.1	12.4
Na_2O	4.07	3.57	2.96	2.86	2.15	1.81	2.06	3.06	2.97		2.57	3.15	3.23	3.84	2.2	2.25
K_2O	1.76	3.52	2.48	4.87	4.63	3.36	4.84	4.96	4.04		3.99	3.84	3.52	3.16	0.5	1.04
P_2O_5	0.13	0.13	0.07	0.13	0.06	0.08	0.11	0.06	0.05		0.09	0.02	0.12	0.06	0.17	0.29
H_2O																0.11
LOI	0.01	0.01	0.01	0.01	0.01	0.01	0.01	0.01	0.01		0.02	0.01	0.01	0.02		1.92
Total	99	98.8	98.7	101	98	98.2	98.4	98.4	99.5		99.4	99	98.9	99.4	98.7	99.3
Rb	81.1	159	147	143	291	261	293	262	231	225	225	208	165	128	12.8	41.3
Sr	233	196	82.4	165	103	165	112	59.8	174	251	270	68.7	660	593	139	241
Y	9.65	6.84	32.2	20	39.9	43	22.4	37.1	31.3	40.9	39.3	24.2	28.4	16.3	35.5	34
Zr	182	227	111	78.2	99.1	201	228	107	180	200	232	154	321	355	112	86.6
V	40.5	31.4	83.8	108	30.3	192	43	11.7	32.6	83.7	69.7	19.9	73.1	76.3	335	336
Ba	398	1024	789	1112	676	1163	675	473	1256	991	1218	788	2095	2145	199	409
Be	1.23	1.9	2.46	2.77	1.84	2.79	2.99	4.47	4.05	2.32	2.47	4.13	2.37	2.74		1
Bi	0.02	0.1	0.22	0.07	0.08	0.06	0.06	0.16	0.06	0.08	0.27	0.07	0.1	0.18		
Cd	0.03	0.02	0.05	0.03	0.02	0.05	0.07	0.02	0.02	0.02	0.02	0.05	0.02	0.07		0.1
Co	84.4	46.5	21.9	63.3	82.1	60.4	52.6	9.3	12.3	51	63.5	130	31.4	32.1	62.5	75.4
Cr	13.1	12	29.8	31.1	13.3	49	23.1	7.22	15.1	19.2	15.3	8.07	11.7	11.2		145
Cs	1.57	2.08	6.06	6.02	5.29	1.69	2.48	3.09	2.54	3.74	4.49	1.58	2.22	2.09	3.1	
Cu	3.49	6.99	4.74	5.29	5.75	26.5	13.5	3.88	2.87	28.6	23.4	2.93	25.2	64	50	118
Ga	19.3	20.2	18.3	17.6	14.1	28.2	19.3	16.4	21.7	17.4	16.9	17.5	20.8	20.7	22	21.9
Ge	0.97	0.71	18.3	1.02	14.1	3.6	19.3	16.4	21.7	1.61	1.49	1.41	2.1	1.32		
Li	40.8	21.8	41.4	70	33.8	36.8	39.4	47.2	39.9	44.7	41.7	10.5	53.9	33.4		17
Mn	292	354	1223	972	462	1402	430	172	352	744	785	292	885	885		
Mo	0.21	0.12	0.26	0.49	0.41	0.73	0.14	0.4	0.15	1.57	1.04	1.56	1.08	0.52		
Ni	5.17	4.14	13.2	12.8	5.2	22.1	12.2	3.76	6.17	12.9	10.2	2.67	7.37	6.49	65	86.8
Sb	0.04	0.06	0.04	0.07	0.09	0.1	1.18	0.06	0.07	0.17	0.18	0.11	0.18	0.27		
Sc	4.91	2.98	11.3	14.7	5.7	25.7	8.27	2.68	5.34	10.7	9.56	5.02	8.65	6.59		
Sn	0.85	1.09	1.24	1.89	1.96	0.91	1.09	3.26	1.9	1.72	1.68	1.32	1.36	1.15		1.14
Tl	0.47	0.88	0.91	0.72	1.27	1.15	1.26	1.25	0.93	0.74	0.92	0.78	0.51	0.81		0.44
Zn	45.5	70	80.7	76.5	35.5	164	69.1	25	46.7	60.5	50.7	35	51.5	112	115	100
La	27.8	35.5	34	33.7	51.7	71.1	81.3	101	91.5	58.4	54	34.9	53.1	32.8	13.5	19.1
Ce	54.6	71	91.7	72	112	158	197	114	157	122	120	68.7	109	83.9	30	34.8
Pr	4.86	6.27	7.72	6.66	12.1	16.6	21.1	21.4	16.2	11.6	12	6	11	6.92	3.9	3.8
Nd	16.9	20.7	27.4	25	43.4	63.5	78.5	79.7	56.7	40.9	42.2	18.6	39	24	17.5	17.3
Sm	3.03	3.81	6.45	5.3	10.3	14.2	17.9	16.4	9.66	8.52	8.82	3.89	7.64	5.06	4.9	4.44
Eu	0.5	0.79	1.22	1.36	1.15	2.88	1.4	1.85	1.62	1.5	1.44	0.67	2.17	1.45	1.8	1.51
Gd	2.1	2.21	5.41	3.92	8.13	11.4	11.1	12.8	6.92	6.35	6.31	2.81	5.23	3.39	6.3	4.84
Tb	0.35	0.37	1.07	0.74	1.83	1.8	1.59	1.89	1.3	1.23	1.23	0.52	0.94	0.54		0.83
Dy	1.95	1.27	5.6	3.59	8.1	8.49	5.51	7.76	5.39	5.63	5.92	3.11	4.4	2.9	6.8	5.2
Ho	0.23	0.18	0.97	0.59	1.39	1.36	0.76	1.03	0.84	1.06	1.05	0.54	0.75	0.43	1.4	0.98
Er	0.61	0.47	2.93	1.63	3.59	3.64	1.92	2.72	2.44	2.99	3.03	1.98	2.07	1.46	4.5	2.74
Tm	0.1	0.08	0.61	0.26	0.54	0.52	0.3	0.37	0.35	0.48	0.49	0.38	0.37	0.26		0.18
Yb	0.5	0.48	3.56	1.73	2.97	3.35	1.57	2.14	2.21	2.99	3.09	2.65	1.88	1.58	4	3.4
Lu	0.12	0.07	0.63	0.3	0.52	0.5	0.29	0.44	0.34	0.52	0.59	0.48	0.34	0.31	0.7	0.49
Hf	3.36	5.1	3.06	1.62	3.08	4.93	6.34	3.36	5.02	4.68	5.24	4.07	6.35	7.17	3	2.86
Ta	2.93	2.28	0.37	1.28	3.93	1.5	2.72	0.86	1.61	1.97	2.76	5.55	1.59	0.59	3	1.27
Nb	9.1	10.3	6.09	5.74	17.7	17.7	18.4	18.1	42.8	22.3	24.8	23.3	19.4	12.7	6	7.82
W	53.5	30.2	5.23	27.1	51	22.9	35.6	7.2	7.98	26.6	35	80	17.7	11.4	46	13
Pb	10.1	19.8	18.2	9.71	31.9	29.4	51.9	81.2	22.7	18.3	16.6	18.8	15.6	61.6		9.69
Th	9.93	15.6	10.6	5.61	33.2	18.6	68.8	12.7	30.1	30.1	33	16.1	13.2	9.89	1	3.81
U	0.74	1.4	2.11	1.81	2.64	0.95	2.97	3.47	2.2	3.93	3.49	1.84	1.98	2.12		0.53

Table 2 (*Continued*)

	ID														
	KV5	*KB5*	*KB9*	KV8	KV7	*KB8*	*KB4*	*KB6*	*KB7*	*IS19*	*IS10*	*IS20*	*IS21*	*IS22*	*IS23*	*IS24*
Type	G_{1c}, bas	G_{1c}, bas	G_{1c}, bas	G_{1c}, bas	G_{1c}, bas	G_{1c}, bas	G_{1c}, bas	G_{1c}, bas	G_{1c}, bas	G_{1c}, bas	G_{1c}, rhyol	G_{1c}, rhyol	G_{1c}, rhyol	G_{1c}, rhyol	G_{1c}, rhyol	G_{1c}, rhyol
Age (Ma)		1871										1856				
SiO_2	48.1	48.5	49.6	51.3	49.2	49.9	51.4	52.2	53.8	54.1	69.3	71.7	73.4	76.2	67.9	77.4
TiO_2	1.05	0.64	2.48	1.73	0.75	0.7	0.67	1.23	1.65	0.99	0.6	0.54	0.78	0.35	0.72	0.35
Al_2O_3	15.4	18.7	14.2	13.1	16.9	18.4	17.1	14.5	13.1	21.7	15.1	14.6	13.3	11.6	16.3	11.3
Fe_2O_3	12.1	6.84	12.7	13.3	9.57	7.13	7.83	10.9	12.6	6.69	4.23	3.13	2.74	1.73	4.53	2.18
MnO	0.17	0.09	0.27	0.2	0.16	0.12	0.11	0.19	0.2	0.08	0.03	0.03	0.03	0.02	0.05	0.02
MgO	7.72	5.53	5.51	6.34	8.19	6.68	7.5	6.17	4.44	1.84	0.97	0.66	0.57	0.3	1.2	0.4
CaO	10.3	10.9	10.2	8.55	10.3	10.6	11.2	8.92	8.97	2.52	2.42	0.61	0.45	0.31	0.86	0.66
Na_2O	1.89	3.74	2.22	3.51	2.42	2.27	2.89	3.68	2.92	4.65	2.2	2.04	4.19	3.19	1.88	2.62
K_2O	0.54	0.53	0.84	0.48	0.4	0.4	0.59	0.06	0.32	4.39	3.15	3.77	2.54	3.74	4.67	2.16
P_2O_5	0.11	0.39	0.15	0.19	0.05	0.36	0.3	0.25	0.22	0.19	0.41	0.25	0.18	0.45	0.08	0.27
H_2O		0.07	0.11			0.14	0.11	0.06	0.1	0.19	0.23	0.19	0.2	0.11	0.25	0.18
LOI		1.78	0.98			2.09	1.44	1.12	0.73	1.32	1.73	1.36	0.79	0.7	1.84	0.88
Total	97.4	97.8	99.3	98.7	98	98.7	101	99.2	99	98.7	100	98.9	99.1	98.7	100	98.5
Rb	18	22.4	29.7	16	10.8	13.1	21.7	1.27	5.28	289	192	171	104	114	299	115
Sr	149	173	167	120	251	275	183	149	102	258	155	98	121	163	165	149
Y	21.5	21.9	61.2	34	16.5	20	22.9	32.5	38.6	39	30.2	35.6	54.4	34.4	50.8	40.4
Zr	81	64.5	147	142	68	14	15.3	19.9	42.8	180	255	156	309	131	204	144
V	230	221	432	285	190	198	240	328	374	132	105	60.3	60.6	42.9	98.9	50.2
Ba	212	240	459	251	141	175	299	46.4	82.3	1074	1088	1077	1089	1321	1301	807
Be		0.71	1.33			0.62	0.75	0.9	1.16	6.58	2.85	2.93	1.8	1.99	3.94	3.3
Bi										0.72	0.2	0.19		0.22	0.34	0.36
Cd		0.08	0.17				0.07		0.11	0.07	0.13	0.07	0.15	0.06	0.1	
Co	61	65.1	80.6	51	46	59.6	73	68.7	80.7	28.4	31.9	29.7	52.3	35.6	50.8	49.8
Cr		594	206			558	666	105	36.1	111	124	41.4	39.7	27.2	138	31.4
Cs	4			8.8	0.5											
Cu	60	86.6	124	95	65	83.8	155	133	113	14.2	21.6	34.7	10.8	15.1	69.3	25.7
Ga	18	17	21.9	16	18	15.5	16.4	16	18.1	27.6	20	16.5	14.7	13.4	24.5	14.2
Ge																
Li		22.3	21.9			23	17.9	13	11	41.9	43.2	22.1	9.76	15.8	41.3	18.2
Mn																
Mo			0.5						0.21		0.26					
Ni	130	120	93.2	40	80	105	118	53.6	36.2	37.5	12.5	10.9	11.9	10.4	43.2	11.4
Sb		0.39					0.23		0.13				0.16		0.16	0.26
Sc																
Sn	1	0.82	0.92	1		0.59	0.85	1.08	2.46	2.7	2.59	2.42	3.06	1.84	3.37	2.04
Tl	1.86	0.31	0.27	0.34	1.95	0.51	0.3	0.45	0.5	0.32	0.34	0.43	0.57	0.49	0.72	0.43
Zn	75	72.2	186	95	60	73.5	81.7	103	119	178	75.5	59	37.2	47.2	164	67.7
La	10.5	12.8	31.4	20	10	10.4	13.4	14.5	16.5	48.4	45.6	28.9	87.9	57.8	76.1	62.3
Ce	22.5	24.6	60.6	42.5	21	21.5	26.2	29.5	33.2	95.3	91.3	54.6	168	104	144	81.6
Pr	2.8	2.8	7.01	5.4	2.6	2.52	2.99	3.54	4.13	10.1	9.55	6.31	17.7	10.7	14.8	12.2
Nd	12	13.1	33.3	22.5	11.5	11.8	13.6	17.4	20.2	39.1	38.2	26.1	71.1	42.9	59.3	49
Sm	2.5	3.23	8.54	5.4	2.5	2.93	3.37	4.49	5.4	7.94	7.52	5.6	13.4	8.58	11.7	9.45
Eu	1.1	1.12	2.61	1.6	1	0.92	1.14	1.47	1.77	1.98	1.77	1.49	2.63	1.82	2.61	2.11
Gd	3.7	3.26	9.04	6.6	2.9	2.98	3.51	5.07	5.96	6.37	6.25	4.63	11.2	7.04	9.58	8.08
Tb	2.75	0.54	0.5	0.68	2.71	1	0.57	0.81	0.98	0.69	0.58	0.89	1.02	0.73	1.61	0.97
Dy	3.7	3.42	9.31	6.4	3.3	3.16	3.71	5.28	6.25	6.61	5.07	4.92	9.26	5.69	8.41	6.59
Ho	0.8	0.67	1.75	1.3	0.7	0.58	0.66	0.98	1.18	1.12	0.87	0.99	1.54	0.96	1.47	1.1
Er	2.4	1.8	4.89	3.9	2	1.62	1.86	2.69	3.21	3.43	2.42	2.81	4.44	2.65	4.22	3.17
Tm	0.93				0.96		0.11			0.61	0.51	0.81	1.38	0.67	0.54	0.51
Yb	2.5	2.21	6.06	3.8	1.5	1.95	2.17	3.08	3.59	4.68	3.28	3.74	5.86	3.34	5.48	4.14
Lu	0.4	0.34	0.87	0.5	0.3	0.25	0.3	0.4	0.49	0.76	0.48	0.55	0.82	0.49	0.79	0.57
Hf	3	1.94	4.51	4	1	0.54	0.83	1.03	1.61	5.39	6.25	4.49	8.65	4.18	5.93	5.04
Ta	1.5	1.43	1.68	2	1.5	0.87	1.18	1.34	2.06	3.15	3.73	2.47	4.55	1.22	3.88	1.29
Nb	3	6.26	14.7	7	3	3.32	4.9	6.28	9.38	30	30.2	22.8	35.5	8.44	34.2	11.2
W	31	18.3	13	33	21	13.2	17.5	15.7	23.5	6.72	25.4	21.1	41.1	23.6	22.4	33.6
Pb		5.06	9.32			4.01	4.81	4.39	5.46	55.9	42.5	25.3	11.7	35	37.7	43.7
Th	1	3.49	3.94	4	3	2.66	3.24	2.74	2.79	25.9	20	18.2	37.3	16	24.4	15.4
U		0.35	0.32			0.34	0.4	0.41	0.42	3.86	3.34	2.9	4.31	2.56	3.52	2.84

Table 2 (*Continued*)

	ID															
	IS3	*IS9*	*KB2*	KV1	*LW12*	*LW13*	*LW10*	*SR7*	*ND2*	SER 6-3	SER-6-2C	SER 6-2	*SR6*	*SR12*	SI/98/3	SI/98/2A
Type	G_{1c}, rhyol	G_{1c}, rhyol	G_{1c}, rhyol	G_{1c}, rhyol	G_{1c}, rhyol	G_{1c}, rhyol	G_{2a}	G_{2a}	G_{2a}	G_{2a}	G_{2a}	G_{2a}	G_{2a}	G_{2a}	G_{2b}	G_{2b}
Age (Ma)					1879		1610		1627	1652	1664			1639		
SiO_2	76.1	72.9	62.1	63.8	76.1	70.6	70.2	69.4	71.9	72.2	72.6	73	74.3	77.3	75.4	72.4
TiO_2	0.49	0.59	0.82	0.76	0.42	0.44	0.58	0.51	0.3	0.28	0.42	0.37	0.3	0.33	0.21	0.26
Al_2O_3	11.5	13.3	22.4	18.7	12	14.9	14.1	13	12.8	12.6	12.4	13	12.7	12.5	12.5	13.7
Fe_2O_3	2.78	4.07	5.89	6.93	1.78	2.78	2.79	4.1	2.76	2.89	4.04	3.78	2.61	2.04	1.46	1.96
MnO	0.02	0.03	0.02	0.03	0.03	0.03	0.03			0.05	0.09	0.08			0.07	0.04
MgO	0.64	0.96	0.84	1.14	0.28	0.4	0.4	0.28	0.24	0.27	0.22	0.26	0.05	0.16	0.13	0.35
CaO	0.63	0.37	0.15	0.24	0.73	1.03	0.83	2	1.31	0.98	1.17	1.36	0.87	0.73	0.55	1.16
Na_2O	2.12	1.54	0.44	0.75	2.2	2.72	2.18	3.49	3.52	2.95	2.7	2.75	2.69	2.21	2.59	3.26
K_2O	2.36	3.35	4.24	3.51	4.3	5.42	6.53	6.38	4.69	5.43	6.02	5.55	4.82	5.26	5.54	4.82
P_2O_5	0.41	0.25	0.16	0.04	0.29	0.19	0.39	0.08	0.09	0.01	0.05	0.05	0.05	0.06		0.07
H_2O	0.21	0.31	0.08		0.14	0.18	0.17									
LOI	1.14	2.21	4.12		0.46	0.54	0.56	0.01		0.45		0.33		0.01	0.23	0.72
Total	98.4	99.9	101	95.8	98.7	99.3	98.8	99.2	97.7	98.1	99.7	100	98.4	101	98.7	98.8
Rb	118	151	225	198	125	147	292	267	172	300	209	241	310	329	406	258
Sr	136	98	78.4	68.6	172	256	77.6	69	86.4	19.1	72	72.7	16.3	24.1	24	127
Y	25.7	24.1	26.2	24.5	27	65.9	64.2	101	96	137	82.5	74	311	88.6	34	19
Zr	155	170	311	220	155	393	288	408	77.3	453	637	501	386	339	184	192
V	78.5	78.9	73.3	55	37.3	60.6	33.4	17.1	15		5	5	6.83	13.2	10	20
Ba	751	796	947	640	1418	1749	1456	1375	1169	379	1125	1095	370	448	263	835
Be	2.05	2.14	4.29		1.63	2.6	2.37	6.96	3.69				6.2	3.98		
Bi	0.27	0.28				0.27		0.09	0.03				0.15	0.03		
Cd	0.07	0.09	0.13		0.09	0.23	0.11	0.57	0.02				0.08	0.03		
Co	43.1	28.7	25.7	20.5	52.2	63.3	45.3	15.9	40.9	14	19	20	6.78	10.3	47.5	32.5
Cr	87.4	89.5	152		18.2	36.6	11.5	7.83	6.92				6.37	7.08		
Cs				3.6				0.77	1.78	2.2	0.8	1.3	1.19	1.82	3.2	1.2
Cu	18.9	32.8	9.03	20	10.2	28.9	12.8	12.8	3.23	5		25	13.8	2.6	15	15
Ga	14	15.3	26.3	27	12.6	18.6	16.7	28.9	24.8	24	23	24	21.2	19.5	17	22
Ge								28.9	24.8				21.2	19.5		
Li	33.2	27.1	57.9		19.9	31.2	87.5	9.46	18.5				6.46	16.5		
Mn								1234	535				563	455		
Mo		0.23						0.64	1.92				0.8	0.96		
Ni	19.9	16.8	36.8	25	6.95	12.7	5.49	2.78	2.13	5	5	5	3.22	2.58		
Sb	0.42					0.35		0.05	0.11				0.04	0.03		
Sc								8.3	10.2				2.11	2.6		
Sn	1.76	1.97	4.86	4	1.93	3.83	5.78	9.6	2.81	6	4	5	7.56	6.26	12	2
Tl	0.7	0.53	0.39	0.5	0.4	0.12	0.18	1.25	0.64	0.5	2	0.5	1.4	1.47	1	0.5
Zn	61.4	70.7	71.2	60	31.6	55	55.1	617	97.6	90	100	90	219	84.4	70	55
La	28.4	37	65.1	49.5	62.1	111	116	94.1	83.2	212	217	102	207	118	67.5	141
Ce	54.4	72.2	136	114	101	210	185	306	175	306	314	200	409	288	130	231
Pr	5.73	7.42	13.7	12.5	11.1	20.9	20.7	22.6	19.2	40.7	50	23.4	41.8	22.5	14.9	28.3
Nd	23.5	29.8	51.4	44	44.7	83.5	80.6	90	71.4	145	183	91	152	80.3	49	94.5
Sm	4.68	5.74	9.5	7.9	8.54	15.6	15.3	20.9	16.4	25.1	31	17.3	39.8	16.8	8.1	12.7
Eu	1.19	1.29	1.82	1.4	1.85	3.11	2.14	2.97	2.52	2.6	3.5	2.4	3.33	1.43	0.7	1.2
Gd	3.87	4.72	7.02	7.1	6.77	13.3	12.8	17.7	14.8	24.4	29.7	15	45.1	15.1	6.8	8.4
Tb	1.4	1.1	0.97	1.97	0.98	0.35	0.95	3.66	2.98	4.4	3	2.7	10.5	2.9	1.1	1.1
Dy	3.78	4.04	5.41	5.4	4.79	11.1	10.7	19	16.9	20.9	20.3	13.6	54	15.6	5.9	3.4
Ho	0.72	0.68	0.83	1.1	0.75	1.88	1.82	3.21	2.86					2.87		
Er	2.06	1.84	2.33	3.4	2.07	5.3	5.14	9.73	8.67	13.2	10.2	7.5	29.6	8.69	3.3	1.7
Tm	1.26	0.53	1.05	1.64	0.52	1.57	1.46	1.7	1.43	1.9	0.93	1.1	4.9	1.59	0.4	0.1
Yb	2.86	2.33	3.19	3.1	2.54	6.91	6.17	9.7	8.63	11.1	8	7	32.1	9.49	3.4	1.2
Lu	0.42	0.35	0.46	0.5	0.36	1	0.91	1.65	1.51	1.7	1.1	1.1	5.24	1.46	0.5	0.1
Hf	4.61	4.6	7.02	7	4.69	11.7	8.16	11	2.32	15	18	14	12.6	10.4	7	6
Ta	1.91	2.69	6.35	3.5	2.67	4.89	3.59	2.21	1.73	8	9.5	8.5	2.06	2.24	11.5	8
Nb	33.3	22.5	79.8	17	20	36.8	30.2	70.7	25.7	61	43	47	81.3	66.8	25	16
W	25.2	19.9	12.7	37	37.1	54	38.8	14.4	25.4	147	176	175	7.2	11.4	261	198
Pb	28.4	24.8	18.8	15	26	39.8	44.1	55.5	18.8	35	30	30	45.7	40	115	40
Th	20	15.8	37.3	31	19.4	66.9	34.3	31.8	15.6	33	35	23	39.4	34.9	49	93
U	2.93	2.66	4.42	4.5	2.09	7.27	2.06	2.9	3.05	2.5	2	1.5	3.87	2.83	6	3

Table 2 (*Continued*)

	ID															
	ML2	*CHT4*	*ND4*	*KTB1*	*CHT6*	SER 5-3	*CHL2*	*MK2*	*KN5*	*CHL4*	*CHT1*	*CC5*	SI/98/11	*KN2A*	*CHL5*	*CC8*
Type	G_{2b}	G_{4A}	G_{4A}	G_{4A}	G_{4A}	G_{4A}	G_{4A}	G_{4A}	G_{4A}	G_{4A}	G_{4A}	G_{4A}	G_{4A}	G_{4A}	G_{4A}	G_{4A}
Age (Ma)	1551		1030		1005	1034			1053			1038		1031	1016	1035
SiO_2	77.3	77.9	68.1	76.9	73	72.5	72.4	76.5	68.8	76.2	71.1	73.4	72.3	72.1	69.8	74.1
TiO_2	0.26	0.07	0.26	0.12	0.84	0.14	0.41	0.11	1.05	0.11	1.37	0.72	0.32	0.48	1.32	0.45
Al_2O_3	11.9	13.1	11.6	13.6	12.7	13.9	12.5	13.4	13.8	13.6	12.4	13.6	12.7	13.4	14.3	13.1
Fe_2O_3	1.43	0.75	3.43	0.87	5.2	1.1	3.49	0.69	5.24	0.79	5.91	4.12	2.72	2.46	5.13	2.04
MnO						0.03							0.04			
MgO	0.16	0.14	3.74	0.18	0.69	0.43	0.22	0.27	1.31	0.21	1.07	0.7	0.19	0.35	1.04	0.48
CaO	1.08	0.51	5.56	0.58	1.77	0.99	1.8	0.79	2.96	0.66	3.42	2.41	1.16	1.8	3.27	1.62
Na_2O	2.3	3.51	4.31	2.43	2.61	2.43	2.92	2.6	2.64	3.26	2.48	2.95	2.83	2.63	2.69	2.84
K_2O	4.18	4.31	1.61	4.46	3.64	5.3	4.71	4.52	3.31	4.36	3.47	3.72	5.47	4.85	3.36	3.84
P_2O_5		0.13	0.24	0.06	0.18	0.18	0.13	0.11	0.1	0.15	0.14	0.15		0.11	0.21	0.06
H_2O																
LOI	0.01	0.01	0.01	0.01	0.02	1.06	0.01	0.02		0.01	0.01		0.33		0.01	0.01
Total	98.6	100	98.8	99.1	101	98.1	98.6	99	99.3	99.3	101	102	98.1	98.2	101	98.5
Rb	494	301	41.1	336	205	329	246	254	177	255	131	116	211	203	186	168
Sr	37.8	54.7	146	55.8	126	64.2	101	74.9	118	59.5	153	194	45.9	131	150	171
Y	24.4	36.9	42.2	40.3	61.4	18	116	15.9	33.1	17.7	61.3	20.8	124	39.8	33.8	38.6
Zr	401	53.9	75.7	158	52.7	43	74.3	122	63.6	101	52	84.7	392	117	96.7	126
V	21	12.7	88.8	16.1	46.5	10	16.9	15	92.9	12.6	44.2	62.8	10	23.2	82.6	38.3
Ba	387	277	290	253	960	327	1695	331	944	427	1650	1762	669	1643	1392	1099
Be	6.67	8.22	3.47	2.55	3.54		4.19	3.89	3.2	6.09	3.61	2.76		3.11	5.33	3.54
Bi	0.07	0.16	0.05	0.08	0.11		0.06	0.03	0.12	0.06	0.09	0.05		0.05	0.13	0.05
Cd	0.04	0.05		0.01	0.05		0.05	0.01	0.03	0.01	0.03			0.02	0.02	0.02
Co	101	56.2	49.5	67.2	55.7	25	71.8	12.7	24.7	59.2	18.1	17.6	19	16.7	53.8	13.5
Cr	9.78	8.46	9	9.05	16		9	8.6	24.9	9.41	8.5	12		8.77	14.4	12
Cs	4.27	10.3	0.26	10.9	3.95	7.2	1.36	3.74	5.45	5.32	2.51	1.51	0.7	2.71	7.31	1.35
Cu	6.09	3.1	2.3	15.5	23	5	5.55	12.8	14.8	2.7	7.51	12.9	5	5.54	15.2	6.54
Ga	26.7	20.9	17.4	12.4	20.5	12	21.1	10.3	19.8	15	19.7	18.7	24	20.7	22	17.7
Ge	1.95	20.9	1.25	0.65	20.5		21.1	0.53	19.8	15	19.7	18.7		1.5	22	17.7
Li	119	24.3	22	49.9	40.6		10.3	30.7	41.9	77.7	43.9	29.3		32.4	120	19.8
Mn	515	563	975	348	794		597	384	859	241	996	608		451	982	427
Mo	2.64	0.36	0.14	0.38	0.44		0.29	0.17	0.57	1.39	0.82	0.7		0.81	0.7	0.36
Ni	4.53	2.95	6.73	3.13	6.38		4.14	1.8	10.7	2.95	3.78	4.4		2.78	6.7	3.53
Sb	0.1	0.1	0.1	0.09	0.03		0.04	0.06	0.09	0.03	0.04	0.04		0.07	0.05	0.05
Sc	6.06	4.99	5.78	3.44	11.1		8.16	2.06	11	1.98	13.1	9.53		8.29	10.1	5.69
Sn	6.16	1.31	0.86	2.98	2.65	5	5.37	1.88	1.09	1.4	0.96	0.97	4	1.29	1.32	1.37
Tl	1.79	1.37	0.23	1.42	0.93	0.5	1.17	1.05	0.75	1.02	0.6	0.54		0.97	1.01	0.68
Zn	77.2	24.5	109	24.8	85.3	10	96.9	19	79.1	24.7	118	95.5	75	59	116	50.3
La	118	18.5	23.2	18.2	57	17	129	13.9	44	23.2	81.6	29.8	159	47.6	52.1	75.6
Ce	244	30.4	67.9	39.1	121	34.5	180	30.3	108	42.9	176	73.2	232	117	118	154
Pr	23.2	3.21	8.09	5.48	13.3	3.9	25.7	3.25	9.58	3.83	20.4	7.27	34.4	10.3	12	14.6
Nd	78.9	11.6	33.6	23.4	51.3	14.5	98.5	10.8	35.6	13.8	81.6	27.6	132	37.6	45.9	50.6
Sm	15.1	3.28	7.95	6.14	12.6	2.7	20.5	2.84	7.94	3	16.5	5.89	23.9	8.42	10.1	10.1
Eu	0.7	0.59	1.14	0.99	1.93	0.5	3.19	0.58	1.52	0.47	2.77	1.56	3.6	2.14	2.14	1.41
Gd	10.8	3.46	6.86	5.82	10.7	2.9	20.2	2.12	6.06	2.59	13.5	4.61	25.1	6.96	7.56	7.06
Tb	1.75	0.82	1.39	0.98	2.11	0.4	3.72	0.43	1.14	0.61	2.37	0.78	4.1	1.2	1.38	1.26
Dy	6.42	4.47	7	5.41	10.9	2.3	19	2.32	5.37	2.58	12.6	4.24	20	6.04	6.88	6.28
Ho	0.8	0.98	1.17	1	1.89	0.5	3.33	0.38	0.97	0.47	1.85	0.69	4.2	1.06	1.01	1.04
Er	1.74	2.93	3.27	2.46	5.24	1.6	10.3	1.13	2.8	1.47	5.66	1.99	11.5	3	2.88	3.17
Tm	0.24	0.55	0.63	0.43	0.89	0.3	1.62	0.17	0.5	0.22	0.92	0.27	1.6	0.45	0.46	0.6
Yb	1.24	3.4	4.01	2.86	6.06	1.6	10.1	0.98	2.99	1.45	5.02	1.75	9.2	2.75	2.99	3.88
Lu	0.24	0.64	0.76	0.43	0.86	0.2	1.57	0.19	0.55	0.27	0.89	0.34	1.5	0.49	0.49	0.62
Hf	10.4	2.13	2.15	2.61	1.75		3.11	2.23	1.61	2.7	1.79	2.11	12	2.96	2.48	3.45
Ta	5.02	4.32	1.44	2.96	2.1	9	3.62	0.72	0.35	2.95	0.51	0.44	9.5	0.86	0.55	0.56
Nb	73.3	21.6	7.77	18.8	16.7	7	28	5.97	5.12	14.7	12.2	12.9	45	19.9	6.58	10.6
W	59.6	39.8	17.5	40.6	34.6	235	50.8	10.1	3.88	44.9	6	7.04	187	12.2	18.7	4.54
Pb	42.9	42.1	3.62	31.5	33.4	35	48.4	30.9	19.1	40.7	31.7	26.3	20	27.3	27.6	17.7
Th	58.2	11.9	13.9	6.09	16.9	8	33.8	7.06	12.4	13.1	22.8	5.02	15	12.8	9.83	20.1
U	5.4	7.08	1.15	2.4	1.66	3	1.71	1.63	3.26	5.49	2.01	1.39	1	1.5	2.06	2.68

Table 2 (*Continued*)

	ID															
	CHT2	*MH4*	MQG-1	MGG-2	*MUN*	*SR5*	*MK7*	*KK1*	*FW1*	*SR9*	MTG-5	*KN7*	*SH9*	SER 6-6	*ND5*	MTGG-3
Type	G_{4A}	G_{4A}	G_{4A}	G_{4A}	G_{4A}	G_{4A}	G_{4A}	G_{4A}	G_{4A}	G_{4A}	G_{4A}	G_{4A}	G_{4A}	G_{4A}	G_{4A}	G_{4A}
Age (Ma)		1017			1025		1035	1003	1038			1048			1028	
SiO_2	67.6	74.6	74.6	74	75.1	68.9	73.2	68.8	70.5	70	74.8	75.3	74.6	66.5	64.6	72.2
TiO_2	0.65	0.53	0.13	0.17	0.23	0.73	0.27	0.51	0.67	0.64	0.16	0.21	0.68	0.52	0.82	0.27
Al_2O_3	15.5	12.4	13.1	13.2	13.2	14.6	14.6	14.9	15.4	14.9	14	13.7	12.1	16	14.4	14.1
Fe_2O_3	5.87	3.63	1.67	2.04	2.13	4.49	1.43	3.74	3.87	3.33	1.38	1.33	2.51	4.29	4.77	2.23
MnO			0.04	0.04		0.05					0.04		0.04	0.09		0.01
MgO	2.18	1.54	0.11	0.15	0.11	0.79	0.41	0.33	1.18	0.69	0.29	0.28	0.38	1.62	2.48	0.94
CaO	1.23	2.71	0.79	0.79	0.88	1.93	0.49	2.65	2.44	2.37	1.21	0.89	1.31	3.87	2.7	0.3
Na_2O	1.87	1.86	3.28	3.08	2.58	2.26	3.63	2.08	2.77	3.28	3.36	2.71	2.75	3.27	3.08	2.36
K_2O	3.38	1.89	6.13	6.29	5.11	6.25	5.18	4.85	4	4.25	4.88	4.36	3.12	2.83	5.87	6.7
P_2O_5	0.13	0.04			0.07	0.33	0.08	0.14	0.12	0.1	0.09	0.11	0.28	0.5	0.1	0.09
H_2O													0.18			
LOI	0.02					0.01	0.01	0.01	0.01	0.01		0.01	0.54	0.71	0.1	
Total	98.5	99.2	99.8	99.8	99.4	100	99.3	98.1	101	99.5	100	98.9	98.5	100	98.9	99.2
Rb	139	270	210	221	212	261	280	204	252	156	311	285	314	143	361	294
Sr	126	126	25.6	27.6	36	189	87.9	161	291	178	103	105	90.5	282	761	104
Y	24	21.5	48	55	58.4	23.6	20.7	39.4	28.1	19.3	10.5	10.6	48.4	33	41	21.5
Zr	218	269	234	247	176	402	197	127	236	127	105	207	291	181	275	189
V	96	36.1			12	37.2	18.6	29.2	67.5	42.1	10	18.6	22.7	50	185	20
Ba	819	1432	207	253	448	1387	721	1401	1195	967	630	520	638	1165	4595	779
Be	1.31	5.57			2.7	3.01	4.18	3.37	4.06	2.86		2.62	2.44		8.48	
Bi	0.04	0.06			0.08	0.07	0.01	0.12	0.04	0.02		0.04			0.15	
Cd	0.02	0.02			0.03		0.03	0.05		0.02		0.01	0.11		0.03	
Co	29.4	16.1	19	19	49.7	27.5	73.5	75.1	36.3	31.5	12.5	6.57	27.1	22	39	17
Cr	138	11.6			8.73	12.9	7.86	6.97	27.2	12.2		7.7	9.15		56.2	
Cs	3.25	3.65	2.4	2.6	2.89	2.08	1.13	1.17	5.47	2.68	9.2	2.45		4.9	5.94	1.4
Cu	15.2	14.2	5		2.29	12.3	7.4	14	18.1	9.14		2.56	9.31	20	69.8	
Ga	21.2	23.8	23	24	20.7	21.8	19.9	23.7	22.2	17.4	20	17.5	19.1	19	24.5	22
Ge	21.2	23.8			20.7	21.8	19.9	2.25	22.2	17.4		1.18			3.62	
Li	31.2	66.6			31.3	30.8	29.6	24.7	77.4	30.9		56.3	52.8		61.2	
Mn	1606	640			400	508	189	593	507	425		322			1259	
Mo	0.25	0.54			1.14	0.38	0.27	0.44	0.18	0.23		0.04			1.71	
Ni	56.8	4.3	10		2.8	5.84	3.27	3.86	11.6	4.98		3.66	3.93	25	30.7	
Sb	0.12	0.08			0.06	0.05	0.05	0.08	0.04	0.04		0.06			0.19	
Sc	13	3.51			7.34	3.27	4.09	6.74	8.75	6.27		3.03			16.5	
Sn	0.52	2.33	3	4	2.12	1.05	2.11	0.95	4.65	1.28	6	2.31	3.39	4	1.82	7
Tl	0.97	1.55	0.5		1.08	1.44	0.86	1.12	1.13	0.76	0.01	1.18	0.23		0.94	0.23
Zn	107	93	55	75	79.7	85.2	21.7	79.5	70.1	53.3	50	46.9	58.3	40	126	40
La	43.5	53.1	122	137	132	53.6	45.2	83.6	91.5	38.2	39.5	32.1	153	70	126	85
Ce	95.2	129	248	281	285	135	96.7	192	193	81.7	71.5	88.6	301	132	248	159
Pr	8.42	10.6	28	31.6	26.6	13.1	9.67	17.1	17.7	7.98	7.4	6.88	29.9	14.8	24.2	17
Nd	31.8	40.2	104	116	93.6	47.4	34.7	62.1	56.6	29.4	23	24	114	55	84.2	56
Sm	7.33	6.88	18	21.5	19.1	8.73	7.49	11.8	10.4	6.5	3.9	4.94	20.4	10.2	17	8.8
Eu	0.89	1.03	1	1	1.14	1.87	0.75	2.06	1.51	1.58	0.8	0.59	1.37	1.5	4.04	1.2
Gd	5.34	5.09	16.5	19.9	13.8	7.91	5.05	9.27	6.12	4.91	3.5	3.07	15.6	9.7	10.9	8.5
Tb	0.88	1	1.97		2.46		0.93	1.55	0.95	0.96		0.49	0.98	1.4	1.74	0.98
Dy	3.83	4.26	11.4	12.9	11.2	5.24	4.29	6.66	4.75	3.88	2.3	1.7	10.1	6.6	7.28	4.7
Ho	0.62	0.71	2.1	2.3	1.78	1	0.69	1.21	0.75	0.66	0.3	0.26	1.44	0.9	0.95	0.8
Er	2.07	1.9	5.8	6.7	5.16	2.63	1.96	3.22	2.2	1.65	1.2	0.7	3.68	2.5	2.86	2.2
Tm	0.34	0.37	1.64		0.78		0.31	0.49	0.38	0.22		0.1	1.48	0.3	0.53	1.48
Yb	2.08	2.17	4.9	5.4	5.15	2.05	1.72	3.01	2.4	0.98	1	0.74	3.53	1.6	2.78	1.7
Lu	0.38	0.37	0.8	0.8	0.78	0.28	0.3	0.37	0.32	0.18	0.1	0.14	0.47	0.2	0.47	0.3
Hf	5.29	6.76	8	8	5.01	9.39	5.58	2.12	5.87	3.64	3	4.68	8.21	5	5.55	6
Ta	0.6	0.72	9	9.5	2.76	4.77	4.69	2.74	0.89	2.15	7	0.81	4.94	5	1.15	6.5
Nb	14.6	25.3	15	18	23	24.6	30.8	25.1	13	13.1	12	18.6	42.6	10	27.8	19
W	7.24	8.51	184	186	39.2	250	56.1	45.5	11.8	30.7	113	5.18	20.8	113	12.4	141
Pb	23.7	36.4	45	45	35	52.3	17	47.2	48.1	19.5	40	46.3	61.8	35	25.1	65
Th	17.9	12.5	41	45	29.7	47.2	27.1	34.6	50.2	15.4	25	32.8	99.1	23	41	61
U	1.88	1.44	4	4	2.23	1.85	5.59	0.95	3.5	0.86	3	2.55	8.46	4.5	7.2	8.5

Table 2 (*Continued*)

	ID															
	SH8	SER 6-4	*KN4*	*MH5*	*CC4*	SI/98/5	KN8b	*LW1*	*MH9C*	*KN8*	*ND1*	MTG-1	SI/98/6	*LW2*	*LWC*	*LW9*
Type	G_{4A}	G_{4A}	G_{4A}	G_{4A}	G_{4A}	G_{4A}	G_{4A}	G_{4A}	G_{4A}	G_{4A}	G_{4A}	G_{4A}	G_{4A}	G_{4B}	G_{4B}	G_{4B}
Age (Ma)		1036					1022	1005	1029	1022	1023			943		
SiO_2	70.4	66.2	72.5	74.2	75.7	73	72.5	72.4	70.7	69	71.6	73.3	68.3	76.1	73.5	
TiO_2	0.27	0.91	0.69	0.27	0.21	0.22	0.51	0.34	0.46	0.5	0.22	0.26	1.01	0.02	0.03	
Al_2O_3	14	15.1	14.7	14.5	12.8	14.1	14.6	14.5	16.2	15.7	14.5	14	13.9	12.2	16.2	
Fe_2O_3	1.88	5.1	1.61	1.51	1.66	1.39	2.68	1.8	2.07	2.57	1.54	1.7	6.28	0.39	0.56	
MnO	0.01	0.04				0.04		0.02				0.01	0.1			
MgO	0.3	0.84	0.4	0.44	0.29	0.32	0.87	0.34	0.49	0.84	0.15	0.36	1.02	0.01	0.04	
CaO	1.15	2.39	1.24	0.95	0.98	1.37	1.7	0.62	1.64	1.57	0.76	1.33	2.69	0.01	0.63	
Na_2O	2.95	2.37	2.81	2.59	2.75	2.59	2.63	2.71	2.72	2.37	2.73	3.04	2.76	4.78	7.3	
K_2O	5.19	5.31	4.9	3.86	4.21	5.54	4.9	5.13	4.6	5.03	7.59	5.75	3.01	3.98	0.45	
P_2O_5	0.73	0.49	0.23	0.08	0.08	0.01	0.16	0.08	0.12	0.14	0.07	0.08	0.21	0.22	0.32	
H_2O	0.17							0.1						0.1	0.14	0.14
LOI	0.63	0.7	0.01	0.01	0.01	0.5	0.01	0.53	0.01	0.01	0.01		0.53	0.27	0.46	0.57
Total	97.7	99.5	99.1	98.4	98.7	99	100	98.6	98.9	97.8	99.1	99.9	99.8	98.1	99.6	0.7
Rb	303	295	332	195	184	252	261	288	223	241	329	283	235	157	35.5	314
Sr	100	180	151	79	115	174	567	177	168	550	88.2	186	180	10.9	35.7	16.3
Y	24.1	42.5	9.8	6.49	18.4	18.5	31.2	19.9	13.8	38.4	10.7	15	55	7.09	12.8	11.2
Zr	208	346	212	154	189	127	107	270	153	124	112	193	276	8.41	32	33.5
V	18	40	31.6	21.7	22.9	15	55.1	27.8	36.9	56.6	11.7	15	85	13.1	16	11.7
Ba	756	1130	1056	725	1032	822	3685	1360	1347	2854	776	910	866	63.5	56.6	10.9
Be	2.4		7.39	1.26	3.65		5.97	3.46	2.82	5.2	2.03			5.76	13.1	7.15
Bi			0.05	0.08	0.04		0.08	0.16	0.02	0.08	0.01			0.16		0.26
Cd	0.07		0.02	0.01	0.01		0.02	0.12	0.02	0.03						
Co	37.5	22.5	63.8	10.4	11.2	26.5	19	29.9	13	18.2	22.9	13	30	51.5	30.4	61.7
Cr	12.9		9.09	16.8	9.89		24.2	13.8	9.09	22.1	7.1			1.92	0.14	1.45
Cs		3.1	7.19	6.22	1.76	1.6	5.92		2.05	4.77	1.31	2.4	4.3			
Cu	2.58	25	3.72	5.95	3.21	10	8.58	11.4	5.8	7.45	3.05		25	1.09	17.4	1.27
Ga	18.1	23	22.6	15.4	18.3	16	19.9	18.5	18.1	17.8	20	24	24	30.7	12.1	18.2
Ge			22.6	15.4	18.3		19.9		1.54	2.2	20					
Li	50.6		89.6	94.1	34.7		61.3	36.7	24.1	59.5	26.3			1.15	35.1	77.5
Mn			351	288	351		515		388	487	127					
Mo	0.29		0.26	0.14	0.09		0.19		0.16	0.08	0.45					
Ni	8.05		4.19	6.63	2.96		11	4.26	3.85	10.8	2.64			0.87	1.27	1.1
Sb			0.04	0.04	0.05		0.03		0.04	0.04	0.13					0.21
Sc			3.33	1.93	3.82		7.42		5.31	8.46	3.79					
Sn	6.22	3	2.7	1.26	1.6	3	2.32	2.49	0.7	1.94	0.79	1	9	0.63	3.08	12.4
Tl	0.17	0.5	1.8	1.13	0.72	1	1.66	0.78	0.93	1.26	1.2	0.31	0.5	0.82	0.88	0.32
Zn	47.8	75	56.9	42.7	42.3	20	59.5	62	46.2	55.3	25.8	50	85	8.65	10.1	24.3
La	86	131	48.5	25	55.1	71	155	113	68.3	169	51.3	111	163	10.1	5.38	7.64
Ce	161	225	117	56.8	112	141	193	207	127	178	119	213	224	16.3	10.7	13.8
Pr	15.6	28.9	10.3	5.73	11.1	14.9	28.7	20.1	12.5	29.9	11.7	22	34.8	2.29	1.09	1.49
Nd	58.9	107	35.5	21.3	36.5	52.5	106	73.8	39.3	102	41.3	73	128	9.68	4.38	5.35
Sm	10.7	17.1	6.55	4.31	7.01	8.8	18.7	12.4	6.42	19.9	8.05	10.8	18.9	1.78	1.52	2.03
Eu	1.24	2.1	0.9	0.44	0.92	1.2	3.33	1.71	1.33	3.64	1.3	1.5	2.4	0.24	0.2	0.12
Gd	8.11	13	3.36	2.91	5.11	6.5	12	8.67	4.32	12.4	5.25	9	17	1.43	1.57	1.85
Tb	0.3	1.8	0.55	0.49	0.81	0.8	1.8	1.45	0.67	1.89	0.72	0.59	2.5	1.85	1.87	0.86
Dy	4.98	8.2	2.01	1.83	3.63	2.9	7.43	4.52	2.81	7.25	2.89	3.5	11.2	1.19	1.97	1.87
Ho	0.69	1.4	0.25	0.23	0.54	0.4	1.13	0.59	0.34	1.02	0.38	0.6	2	0.18	0.33	0.27
Er	1.73	3.9	0.69	0.6	1.26	1.5	2.81	1.41	1.1	2.7	1	1.7	5.3	0.46	0.91	0.79
Tm	0.21	0.4	0.11	0.08	0.17	0.1	0.37	0.14	0.16	0.34	0.11		0.6	1.53	0.67	0.52
Yb	1.55	2.3	0.83	0.4	0.85	0.9	1.88	1.26	0.71	1.63	0.47	0.9	3.1	0.6	1.49	1.04
Lu	0.22	0.3	0.12	0.11	0.22	0.1	0.22	0.21	0.11	0.22	0.09	0.1	0.4		0.21	0.13
Hf	6.24	9	5.61	4.35	4.93	3	2.71	7.49	3.38	2.69	3.45	6	7	0.41	1.76	1.89
Ta	1.57	6.5	3.92	0.65	1.18	7.5	0.74	1.97	0.59	1.09	1.25	5.5	8	0.74	0.76	1.64
Nb	20.5	28	24.6	12.8	16.9	9	19.7	18.5	12.4	20	9.89	20	24	4.49	0.22	13.3
W	27.3	144	55.9	6.54	7.12	190	11.7	22.9	5.2	9.73	16.9	106	151	33	16	44.4
Pb	54.8	40	62.9	34.8	25.7	70	78.5	52.8	32.6	62.9	42.9	55	30	4.6	23.7	82.5
Th	50.9	48	30.1	18.9	15.4	37	23.2	58.6	21	22.9	38.9	63	53	2.54	3.54	4.9
U	5.98	2	2.73	2.23	2.64	2.5	2.01	3.62	1.62	1.2	2.02	4.5	3.5	0.56	2.64	6.68

Sample ID's in italics were analysed by the first author.

[a] Denotes zircon U–Pb SHRIMP age (De Waele, 2005).

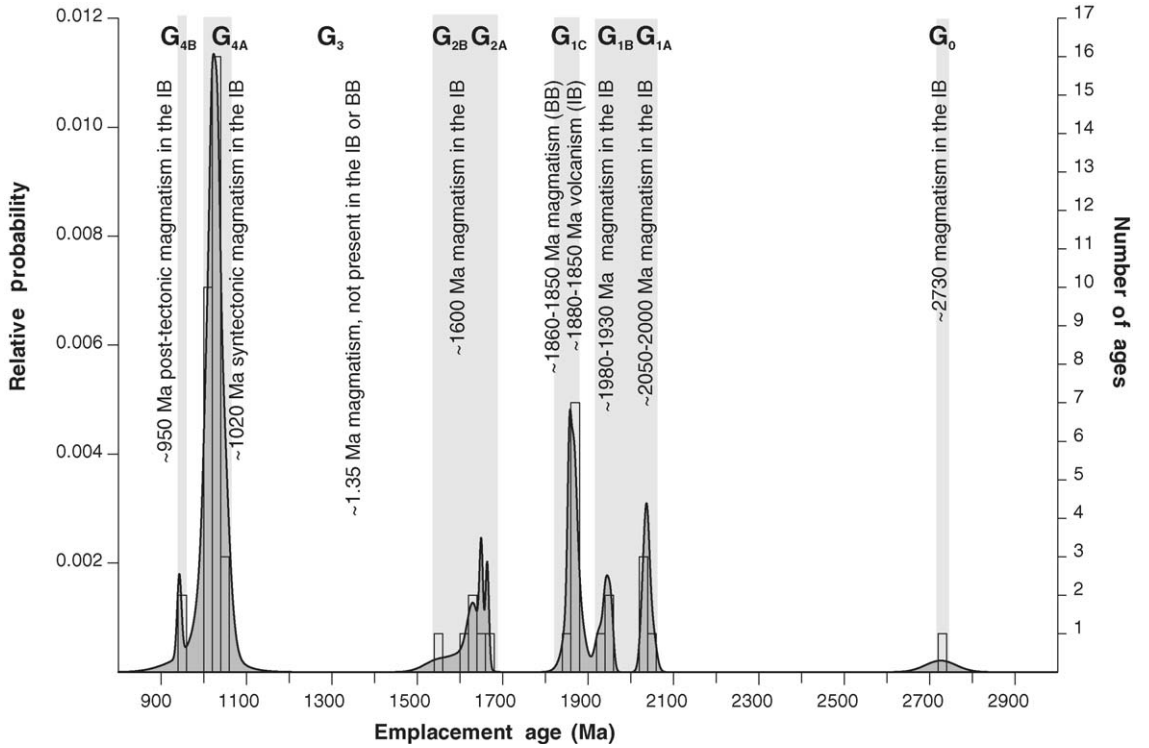

Fig. 3. Combined probability density and histogram diagram (bin size 20 Ma) of age data reported in Table 1b, indicating proposed subdivision of magmatic units in northern Zambia. IB: Irumide Belt and BB: Bangweulu Block.

4.2. Isotopic analysis

After acid dissolution of the sample and Sr and Nd separation on ion-exchange resin, unspiked Sr isotopic compositions have been measured on Ta simple filament (VG Sector 54), unspiked Nd isotopic compositions on triple Ta–Re–Ta filament (VG Sector 54) in the Section of Isotope Geology of the Africa Museum, Tervuren. Repeated measurements of Sr and Nd standards have shown that between-run error is better than 0.000015 (2σ). The NBS987 standard has given a value for $^{87}Sr/^{86}Sr$ of 0.710287 ± 0.000005 (2σ on the mean of 16 standards, normalised to $^{86}Sr/^{88}Sr = 0.1194$) and the Rennes Nd standard a value for $^{143}Nd/^{144}Nd$ of 0.511956 ± 0.000006 (2σ on the mean of 11 standards, normalised to $^{146}Nd/^{144}Nd = 0.7219$) during the course of this study. All measured ratios have been normalised to the recommended values of 0.710250 for NBS987 and 0.511963 for Nd Rennes standard (corresponding to a La Jolla value of 0.511858) based on the four standards measured on each turret together with 16 samples. Decay constant for ^{87}Rb ($1.42 \times 10^{-11}\ a^{-1}$) was taken from Steiger and Jäger (1977) and for ^{147}Sm ($6.54 \times 10^{-12}\ a^{-1}$) from Lugmair and Marti (1978). T_{DM} have been calculated following Nelson and DePaolo (1985) using the Sm and Nd concentrations given in Table 2. The estimated error on the Sm/Nd ratio induces, as a mean, an error of 100 Ma on the T_{DM} model ages, and model ages therefore represent an estimation only of the mean age of the source(s). The degree of preservation of the parental Sm/Nd ratio of the rock depends on the degree of partial melting and nature of the source. If the source was felsic crust, the Sm/Nd will increase, if the source was much more mafic, it will decrease. In the former case, the T_{DM} model ages are valid, in the latter, they represent minimum model ages. The data are shown in Table 3.

5. Results

5.1. The magmatic groups: major, trace elements and Nd isotopes

The Irumide Belt and the Mansa area (western Bangweulu Block) contain a rich record of magmatism spanning the Palaeo- to Mesoproterozoic eras, which can be subdivided into four groups (Table 4; Fig. 3) on the basis of available geochronological data in addition to Archaean relics (subscript 0): Middle Palaeoproterozoic (subscript 1); Late Palaeoproterozoic–early

Table 3
Whole-rock Sm–Nd isotopic data for magmatic rocks in northern Zambia

Suite		Lithology	Sample	Age (T)[a] (Ma)	$^{87}Rb/^{86}Sr$[b]	$^{87}Sr/^{86}Sr$ (2σ)	$^{87}Sr/^{86}Sr$ (T)	$^{147}Sm/^{144}Nd$[b]	$^{143}Nd/^{144}Nd$ (2σ)	T_{DM} (Ma)	$\varepsilon_{Nd}(T)$
G_{1A}	SW Irumide	Granite Gneiss	MK3	2042	2.532	0.760874 ± 0.000014	0.687923	0.1282	0.511250 ± 0.000010	3253	−9.2
G_{1B}	NE Irumide	Granite Gneiss	ISK1	1942	4.614	0.806734 ± 0.000010	0.673804	0.1353	0.511458 ± 0.000011	3134	−7.8
G_{1C}	NE Irumide	Basalt	KB5	1871	0.3743	0.715501 ± 0.000007	0.705429	0.1488	0.511909 ± 0.000012	2691	−2.6
G_{1C}	NE Irumide	Basalt	KB6	1871	0.0247	0.708506 ± 0.000007	0.707841	0.1560	0.512091 ± 0.000012	2536	−0.8
G_{1C}	NE Irumide	Basalt	KB7	1871	0.1498	0.709143 ± 0.000009	0.705112	0.1617	0.512202 ± 0.000013	2483	0.0
G_{1C}	NE Irumide	Basalt	KB8	1871	0.1375	0.709124 ± 0.000009	0.705424	0.1503	0.511904 ± 0.000010	2772	−3.1
G_{1C}	NE Irumide	Basalt	KB9	1871	0.5134	0.717845 ± 0.000016	0.704029	0.1550	0.511868 ± 0.000016	3115	−5.0
G_{1C}	NE Irumide	Rhyolite	IS20	1856	5.099	0.804667 ± 0.000011	0.667449	0.1297	0.511580 ± 0.000010	2674	−4.4
G_{1C}	NE Irumide	Rhyolite	IS23	1867	5.290	0.810731 ± 0.000010	0.668374	0.1197	0.511575 ± 0.000014	2388	−2.1
G_{1C}	NE Irumide	Rhyolite	LW12	1879	2.100	0.755690 ± 0.000009	0.699186	0.1156	0.511456 ± 0.000008	2476	−3.4
G_{1C}	NE Irumide	Rhyolite	LW13	1867	1.661	0.749127 ± 0.000012	0.704433	0.1130	0.511480 ± 0.000012	2372	−2.3
G_{1C}	Mansa	Granite	MA1	1860	2.609	0.762539 ± 0.000009	0.692344	0.1259	0.511457 ± 0.000010	2779	−5.9
G_{1C}	Mansa	Granite	MA2	1862	2.416	0.760835 ± 0.000009	0.695810	0.1264	0.511465 ± 0.000009	2782	−5.9
G_{1C}	Mansa	Dacite	MA4	1872	0.6237	0.717746 ± 0.000007	0.700963	0.1272	0.511418 ± 0.000009	2894	−7.0
G_{1C}	Mansa	Dacite	MA5	1876	1.391	0.736737 ± 0.000009	0.699302	0.1080	0.511319 ± 0.000010	2496	−4.3
G_{2A}	SW Irumide	Granite Gneiss	SR7	1638	11.50	0.960629 ± 0.000013	0.688116	0.1402	0.511514 ± 0.000010	3234	−10.0
G_{2A}	SW Irumide	Granite Gneiss	SR12	1639	42.47	1.479682 ± 0.000012	0.472835	0.1264	0.511429 ± 0.000009	2848	−8.8
G_{4A}	SW Irumide	Granite	ND4	1030	0.8155	0.719010 ± 0.000007	0.706936	0.1432	0.511540 ± 0.000008	3325	−14.4
G_{4A}	SW Irumide	Granite	SR5	1027	7.123	0.781758 ± 0.000009	0.676304	0.1114	0.511286 ± 0.000010	2634	−15.2

Whole-rock Rb–Sr and Sm–Nd isotopic data for magmatic units in northern Zambia.

[a] U–Pb zircon SHRIMP age, see De Waele (2005).

[b] Errors on the $^{87}Rb/^{86}Sr$ and $^{147}Sm/^{144}Nd$ ratios are estimated at 4%.

Table 4
The different magmatic groups of the Irumide Belt and Bangweulu Block

Group	Family	Age (Ga)	Nature	Localisation	Abundance	Phase
0		2.73	Gneissic		Very local	NeoArchaean
1	A	2.04–2.03	Granitic/gneissic	C and SW Irumide	Local	Early Usagaran
	B	1.95–1.93	Granitic	Whole Irumide	Local	Late Usagaran
	C	1.88–1.85	Basaltic	NE Irumide	Local	Ubendian
	C	1.88–1.85	Dacitic	NE Irumide	Local	Ubendian
	C	1.88–1.86	Granitic	Mansa		Ubendian
	C	1.88–1.86	Dacitic tuffs	Mansa		Ubendian
2	A	1.66–1.61	Granitic			Lukamfwa
	B	1.55	Granitic		Very local	Post-Lukamfwa
3		1.36–1.33		Unknown in the Irumide Belt		
4	A	1.05–1.00	Granitic	Whole Irumide	Abundant	Irumide
	B	0.95	Granitic	NE Irumide	Local	Post-Irumide

Mesoproterozoic (subscript 2); mid-Mesoproterozoic (subscript 3); and late-Mesoproterozoic to early Neoproterozoic (subscript 4). Each group is subdivided in families (A–C) when this is justified by an age gap within the considered period.

The earliest magmatism is recorded at ca. 2.73 Ga in the Kapiri Mposhi Granodiorite Gneiss (suite G_0). This Archaean basement is intruded by the Palaeoproterozoic G_1 granitoids of the Mkushi Gneiss Complex in the southwestern Irumide Belt and adjacent Copperbelt, and by broadly coeval granitoids (the Luwalizi Granite Gneiss (LGG), Fig. 1) in the northeastern Irumide Belt. Based on geochronological data, these Palaeoproterozoic granitoids can be subdivided, in the southwestern Irumide Belt, into an earlier G_{1A} suite between 2.04 and 2.03 Ga, and a later G_{1B} suite between 1.98 and 1.95 Ga. This distinction inside the G_1 suite is not possible in the northeastern Irumide Belt, where Palaeoproterozoic basement units are less abundant and only the G_{1B} suite has been recorded. The age of these magmatic events coincides with magmatism recorded in the Usagaran Belt, and we propose to extend this term into the Bangweulu Block and Irumide Belt as early Usagaran (G_{1A}) and late-Usagaran (G_{1B}) suites.

Extensive magmatism, both igneous and extrusive, is recorded in the Bangweulu Block between 1.88 and 1.86 Ga, while in the Irumide Belt, a contemporaneous magmatic event (1.88–1.85 Ga) is recorded only in the northeast by felsic tuffs and minor andesitic and basaltic lavas within the deformed Muva Supergroup (De Waele and Fitzsimons, 2004; De Waele, 2005). We propose the term Ubendian (G_{1C}) suite for this magmatic event, based on its similar time-frame as shear-deformation along the Ubendian Belt.

Localised magmatism is recorded in the Irumide Belt between 1.66 and 1.63 Ga in the southwest, and at ca. 1.61 Ga in the northeast, and is termed the Lukamfwa phase (G_{2A}) after the Lukamfwa Hill type locality in the Serenje 1:100,000 map sheet. In the northeastern Irumide Belt, this magmatism is closely followed by an anorogenic pulse at ca. 1.55 Ga (G_{2B}) which saw the emplacement of the precursor granite to the Lubu Granite Gneiss in the northeastern Irumide Belt. Minor, possibly anorogenic, magmatism has been reported to the east of the Luangwa graben, and includes the Mivula Syenite and Ntendele Metatonalite, dated using the zircon $^{207}Pb/^{206}Pb$ evaporation technique at ~1329 and ~1360, respectively (Vrána et al., 2004). This event (G_3) has, however, not been confirmed in the Irumide Belt and will not be further discussed here. A main magmatic phase, called the Irumide phase (G_{4A}), resulted in widespread intrusion of granitoids between 1.05 and 1.00 Ga, and was accompanied by regional metamorphism dated in low Th/U zircon rim overgrowths at 1.02 Ga (De Waele, 2005). Minor post-Irumide granite plutons were emplaced between 970 and 950 Ma, and make up the G_{4B} suite, for which only one sample has been dated (sample LW2).

Hereafter, we will elaborate on the geochemistry of these magmatic rocks, the intrusion of which spans a period of more than 1 Ga (1.7 Ga if taking into account the G_0 phase). As we will show, the studied magmatic episodes are entirely or mainly crustal in origin. This means that the geochemistry of the studied rocks reflects the nature of the crustal source and of the melting/differentiation processes and not the geotectonic setting in which these rocks originated. Because of this, we will not try to determine their origin by using tectonic

discrimination diagrams, but will instead apply other constraints to speculate on their tectonic setting. The rock names given below are based on the Q′-ANOR diagram (a transformation of the QAP diagram for use with CIPW norm values) of Streckeisen and Le Maître (1979).

5.2. G_0 magmatism

The single G_0 sample dated comes from the Kapiri Mposhi Granodiorite Gneiss unit, which consists of a foliated biotite granodiorite—monzogranite. Zircons from this sample (KMP1; granodiorite) yielded a U–Pb SHRIMP age of 2726 ± 36 Ma (De Waele, 2005). Another sample (MK12; monzogranite) has a very close geochemistry and, although undated, is considered to be another representative of this relic Archaean group. These samples straddle the boundary between granite and granodiorite in the TAS diagram (Fig. 4A), plot clearly in the subalkaline field, are peraluminous (aluminium saturation index (ASI) of 1.23 and 1.44; Fig. 4B) and fall within the S-type granitoid field of the classification scheme of Clarke (1992). The two G_0 rocks are distinguishable in the diagram proposed by Sylvester (1989) (Fig. 4C), plotting at opposite sides of the alkaline granite field. This is due to high contents in Al_2O_3 and Na_2O and low contents in FeO_t and K_2O. Such a signature is reminiscent of Archaean TTG suites, as is their low heavy rare earth element (HREE) content (Fig. 5A) with high La_N/Yb_N ratios (38 and 50), a feature not shown by the other groups studied. The other trace elements are less distinctive and their MORB-normalised spectra are similar and plot close to the reference G_{1A} group (Fig. 6A). The two samples analysed in this study do not allow to precisely determine the palaeoenvironment of this suite, and given the scarcity of confirmed Archaean outcrop in the region, it is unlikely that additional data will become available to allow a full characterisation of the suite. However, a garnet residue would be necessary to explain the low abundance of the HREE. This could suggest an origin through the partial melting of the eclogitic portion of a subducting oceanic plate, although this does not agree with the presence of a Nb negative anomaly, more easily reconciled with mantle melting in the presence of aqueous components (Kleinhanns et al., 2003). Whichever is the case, G_0 magmatism demonstrates the presence of an Archaean basement in the Irumide Belt.

5.3. $G_{1A–B}$ magmatism

In the field, it is impossible to distinguish between the G_{1A} and G_{1B} granite and granitic gneiss suites. Nevertheless, all but one sample studied here have been dated, so there is no ambiguity in our dataset. The four G_{1A} samples come from the Mkushi Gneiss unit in southwestern Irumide Belt. Three are strongly foliated biotite gneiss of syenogranitic (KN6) monzogranitic (MK3) or granodioritic (KN1) composition and one is a mildly foliated pink K-feldspar phyric monzogranite (MK5). Three of

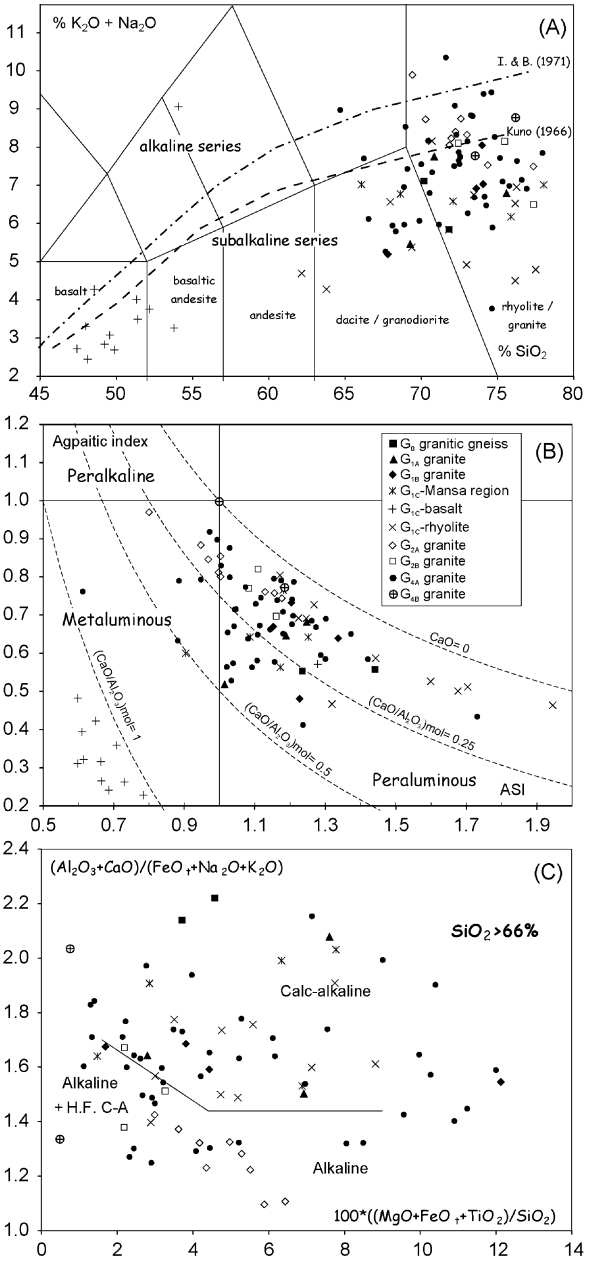

Fig. 4. Major element discrimination diagrams for magmatic rocks of northern Zambia after: (A) Cox et al. (1979) with additional lines after Irvine and Baragar (1971) and Kuno (1966); (B) Maniar and Piccoli (1989); (C) Sylvester (1989).

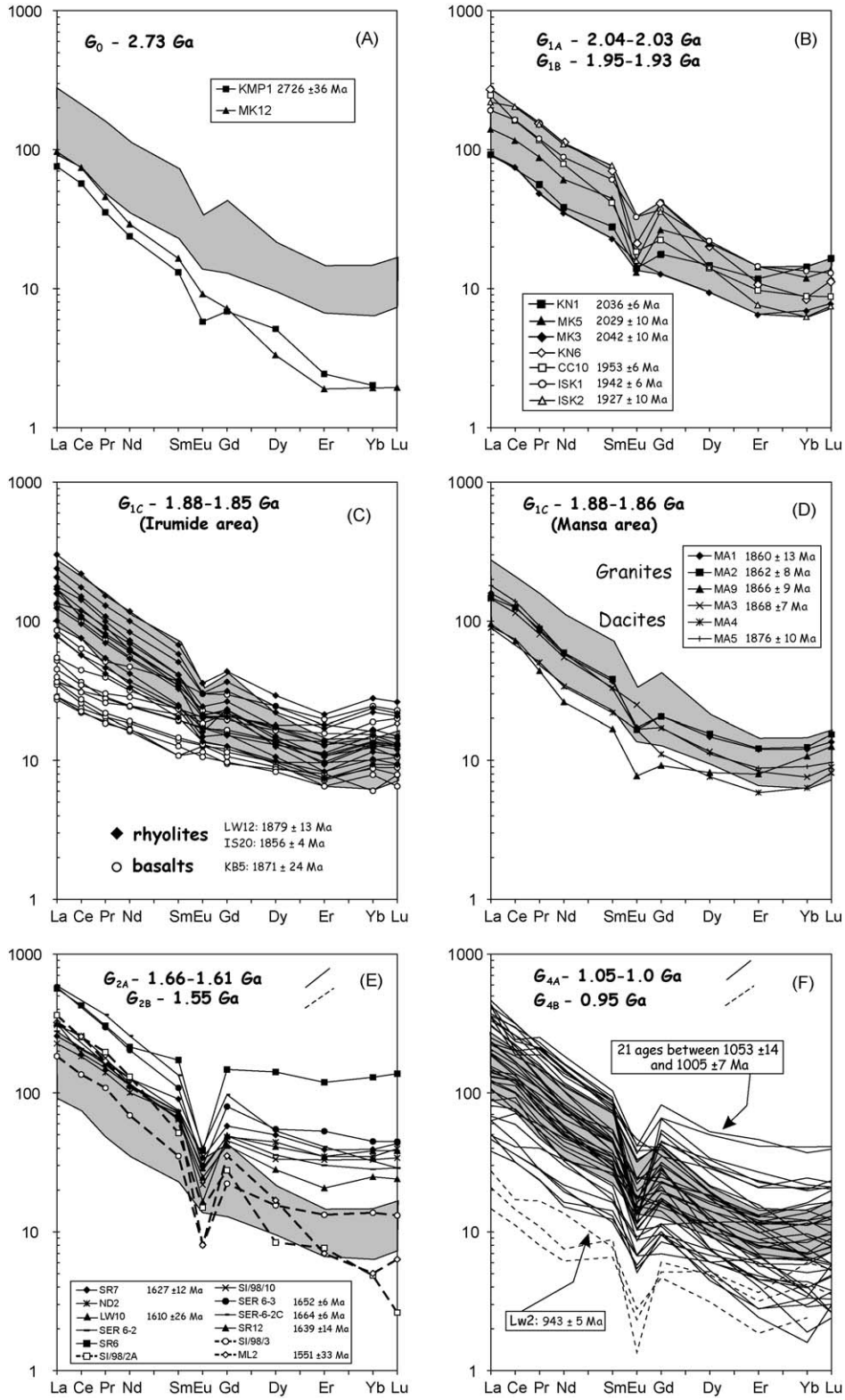

Fig. 5. Chondrite normalised REE plot for magmatic rocks of northern Zambia. Normalising parameters are after Taylor and McLennan (1985); the grey underlying pattern represents the envelope of the $G_{1A–B}$ analyses.

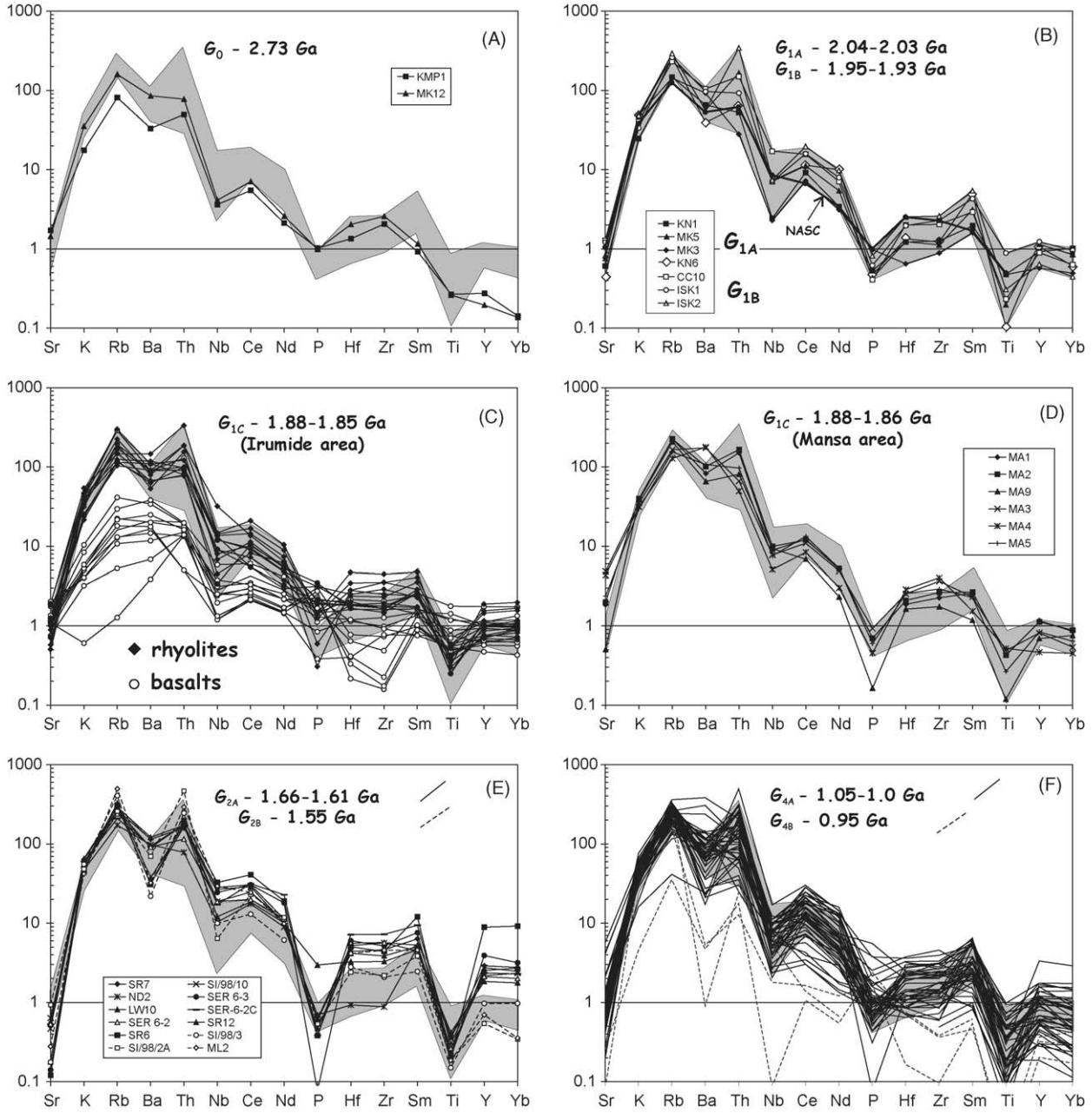

Fig. 6. MORB normalised trace element diagrams for magmatic rocks of northern Zambia, normalising parameters are after Sun (1982); the grey underlying pattern represents the envelope of the $G_{1A–B}$ analyses.

those samples were dated using zircon U–Pb SHRIMP method (De Waele, 2005) and yielded crystallisation ages of 2036 ± 6 Ma (KN1), 2042 ± 10 Ma (MK3) and 2029 ± 7 Ma (MK5). One G_{1B} has been sampled in the same Mkushi unit (monzogranite CC10; 1953 ± 6 Ma; De Waele, 2005). The two other G_{1B} samples were collected from the basement in the northeastern Irumide Belt (Luwalizi Granite Gneiss), which comprises coarse foliated biotite monzogranite (ISK2) and granodiorite (ISK1) and yielded zircon U–Pb SHRIMP crystallisation ages of 1942 ± 6 and 1927 ± 10 Ma, respectively (De Waele, 2005).

Whatever their norm name, all G_1 granitoids are unambiguously subalkaline (Fig. 4A). Their agpaitic index (AI) and aluminium saturation index characterise this group as peraluminous (Fig. 4B), and all but one have

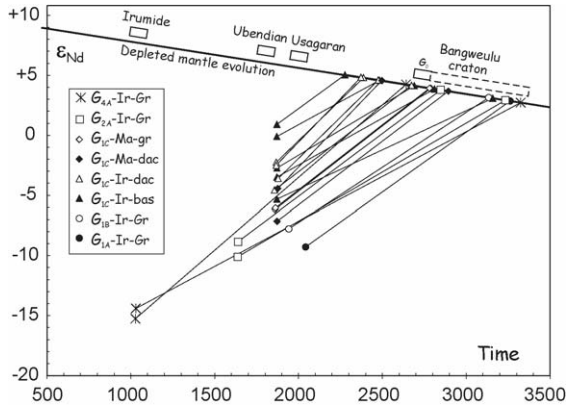

Fig. 7. Initial ε_{Nd} vs. emplacement age diagram for magmatic rocks of northern Zambia.

an ASI > 1.1, which places most G_{1B} granite gneisses in the S-type field in the SiO_2 versus ASI diagram of Clarke (1992). Except KN1 granodiorite, G_1 granitoids have K_2O/Na_2O ratios well over 1 (from 1.3 to 2.3), indicating that both the Mkushi and Luwalizi Granite Gneiss are potassic in nature and globally calc-alkaline (Fig. 4C).

G_{1A} have lower light rare earth elements (LREE) than G_{1B} granitoid gneisses (90–140 and 190–275, respectively; Fig. 5B), lower LREE/HREE fractionation (La_N/Yb_N: 6–13 and 14–35) and lower HREE fractionation (Gd_N/Yb_N: 1.2–2.2 and 2.5–5.7). All samples present a negative Eu anomaly (Eu/Eu^*, G_{1A}: 0.4–0.9; G_{1B}: 0.3–0.7) distinctive of an expected feldspar fractionation. The phosphorous and titanium negative anomalies shown in the MORB-normalised spidergram (Fig. 6B) can be also ascribed to some fractionation, respectively, of apatite and ilmenite or titanite, common in granitoids. The G_1 group shows enrichment in LILE (K, Rb, Ba and Th) and similar concentration of HFS (Hf, Zr, Sm, Y and Yb) with respect to MORB, typical of crust-dominated granitoids (Winter, 2001), and not far from the North American Shale composite (NASC; Gromet et al., 1984).

Both the G_{1A} Mkushi Gneiss (MK3) and G_{1B} Luwalizi Granite Gneiss (ISK1) show low $^{143}Nd/^{144}Nd$ ratios and yielded initial $\varepsilon_{Nd}(T)$ values at −9.3 and −7.8 and T_{DM} model ages of 3262 and 3134 Ma, respectively (Fig. 7). These data support significant crustal residence times and strongly suggest that the Mkushi Gneiss and Luwalizi Granite Gneiss represent reworked Archaean crust. It is noteworthy that these samples, which were collected from opposite sides of the Irumide Belt, display a strong similarity in Nd-isotopic composition, possibly suggesting the presence of an isotopically homogeneous Archaean basement underneath the entire Irumide Belt.

5.4. G_{1C} magmatism

G_{1C} magmatism occurs both on the Bangweulu Craton and in the Irumide Belt (Fig. 1). Whereas, in the Irumide Belt, only extrusive members are reported (basalts, felsic flows and tuffs), coeval granites and felsic flow and tuffs are known on the Bangweulu Block. The association of volcanic and granitic rocks indicates that, on the Bangweulu Block, G_{1C} granites intruded at a shallow level in the crust.

Three samples were collected from the granitoids (samples MA1 (only trace elements), MA2 and MA9) and from the coeval volcanic units (samples MA3, MA4 and MA5) in the Mansa area. The granitoids comprise coarse pink K-feldspar phyric biotite granites and classify as monzogranite. The volcanic units occur either as flows or as volcaniclastic tuffs within the quartzite–pelite succession of the Mporokoso Group; they comprise greenish, fine, sometimes slightly epidotised rocks. Geochemically, two samples are dacitic and one is a rhyolite. Zircon U–Pb SHRIMP crystallisation ages of the three granitic (MA1: 1860 ± 13 Ma; MA2: 1862 ± 8 Ma; MA9: 1866 ± 9 Ma) and two of the volcanic units (MA3: 1868 ± 7 Ma; MA5: 1876 ± 10 Ma) yielded closely clustered ages in keeping with the interpretation that they form part of a single suite (De Waele, 2005). No similarly aged granites have been recognised in the Irumide Belt, but within the deformed metasedimentary succession of the northeastern Irumide Belt, volcanic units have been recognised in three locations. The Katibunga volcanics occur in a fault-bound terrain southeast of Mpika (Fig. 1), and comprise poorly exposed and weathered felsic tuffs and agglomerates and well-preserved dacitic and basaltic units, which locally form pillow lavas (samples prefixed KV and KB, see Table 2). Zircon from a coarse gabbroic dyke associated with the pillow lavas yielded a U–Pb SHRIMP crystallisation age of 1871 ± 24 Ma (De Waele, 2005). A small layer of waterlain felsic crystal tuff has been recognised within a quartzite-sequence in the Luswa River 1:100,000 map sheet (Fig. 1; LW12 and LW13), and yielded a U–Pb SHRIMP zircon crystallisation age of 1879 ± 13 Ma (De Waele, 2005). A 300-m-thick sequence of felsic tuffs, the Kachinga Tuff (Daly, 1995b), occurs within a large isocline south of Isoka (samples prefixed IS, Table 2), and comprises dark-grey waterlain crystal tuffs and massive dacitic flows. One crystal tuff within this succession was dated using zircon U–Pb SHRIMP method at 1856 ± 4 Ma (De Waele, 2005).

The Katibunga volcanic units classify as basalt and basaltic andesite (and one trachite; IS19), while all other volcanic units classify as dacite in the Mansa area and as dacite and rhyolite in the Irumide Belt. Apart from trachite IS19, all volcanic units are subalkaline in composition (Fig. 4A and C). The higher content of Na_2O in KB5, placing it in the alkaline field (Fig. 4A), is most probably not pristine. The Mansa and Irumide G_{1C} felsic units are more scattered but all are also subalkaline (Fig. 4A). Basalts are normally metaluminous, Mansa dacites are moderately peraluminous (ASI up to 1.25), while Irumide rhyolite can be highly peraluminous (ASI from 1.2 to 1.9, with two samples at 3.4 and 4.0) probably due to Na_2O loss.

The REE patterns of the G_{1C} basalts (Fig. 5C) display low to moderate enrichment in LREE (La_N between 25 and 50 (+KB9 at 85); La_N/Yb_N between 2 and 5) and subhorizontal HREE (Gd_N/Yb_N between 1.1 and 1.6). The Irumide rhyolites have similar HREE as the basalts (Yb_N: 9–28 versus 6–25 and Gd_N/Yb_N between 1.0 and 2.2) but are more fractionated in LREE (La_N between 75 and 300; La_N/Yb_N between 5 and 17). The Irumide rhyolite patterns closely mimic the $G_{1A–B}$ granitoids (grey area in Fig. 5C). Both the Mansa granites and dacites display similar REE patterns (Fig. 5D), some being only slightly lower in abundance.

Similar conclusions can be drawn from the MORB-normalised spidergrams (Fig. 6C): the Irumide rhyolites display nearly identical patterns as the $G_{1A–B}$ granitoids. The basalts are lower in abundance and display Hf–Zr negative anomalies and no Ti–P anomalies. The Mansa granites and dacites display parallel patterns slightly lower in abundance but still in the $G_{1A–B}$ range (Fig. 6D). The resemblance in age, major and trace elements between the Mansa dacites and granites and the Irumide rhyolite supports the interpretation that they form part of a single magmatic suite, to which the basalts are linked. The equivalence with the $G_{1A–B}$ signature moreover suggests that they tapped the same regional source.

The $\varepsilon_{Nd}(T)$ values of the Mansa volcanics (−4.3 and −7) and granitoids (−5.9 and −6.0) indicate a significant crustal input in their formation. Their T_{DM} Nd model ages vary between 2.5 and 2.9 Ga (Fig. 7). The Irumide G_{1C} rhyolites are more depleted for the $^{143}Nd/^{144}Nd$ ratios but still in the same range: $\varepsilon_{Nd}(T)$ between −2.1 and −4.4 (four values) and Nd T_{DM} model ages between 2.37 and 2.67 Ga. The basalts, despite their inherent differences, give $\varepsilon_{Nd}(T)$ between 0 and −5 (5 values) and Nd T_{DM} model ages between 2.48 and 2.88 Ga (+1 at 3.16 Ga). These results suggest an increased mixing between an Archaean crustal source at the origin of the $G_{1A–B}$ group, and a juvenile asthenospheric source to generate the G_{1C} melts.

5.5. $G_{2A–B}$ magmatism

G_2 magmatism is known in two areas (Fig. 1), one in the southwestern part of the Irumide Belt (Lukamfwa Granite Gneiss) and the other in the northeastern part (Musalango Gneiss and Lubu Granite Gneiss). The G_2 magmatism was previously mapped as basement in the northeastern Irumide Belt (Daly, 1995a,b). The Lukamfwa Granite Gneiss (samples SR7, SI/98/10, ND2, SER 6-3, SER-6-2C, SER 6-2, SR6 and SR12) comprises coarse foliated K-feldspar phyric biotite syenogranite and alkali-feldspar granite. SHRIMP U–Pb zircon ages range from 1.67 to 1.62 Ga (SER6-2C: 1664 ± 6; SER6-3: 1652 ± 6; SR12: 1639 ± 14; ND2: 1627 ± 12; De Waele, 2005). The Musalango Gneiss (sample LW10) is a strongly foliated biotite alkali feldspar granite dated at 1610 ± 26 Ma (De Waele, 2005). All belong to the G_{2A} group together with SR7, SI/98/10, SER 6-2 and SR6. The Lubu Granite Gneiss (ML2), a coarse, pink, K-feldspar phyric biotite monzogranite dated at 1551 ± 33 Ma (SHRIMP U–Pb zircon, De Waele, 2005), makes up the only dated sample of the G_{2B} group, but based on similarities in geochemistry we have added samples SI/98/3 and SI/98/2A from the southwestern Irumide Belt to this suite.

Most G_{2A} granites are in or close to the alkaline field in the TAS diagram (Fig. 4A) and are metaluminous or slightly peraluminous (ASI from 0.8 to 1.18) with sample SR7 being nearly peralkaline (agpaitic index = 0.97). This alkaline character of the G_{2A} group is also displayed in Fig. 4C; this is the only group plotting entirely in the alkaline field. The G_{2B} group is composed of monzogranite (ML2) and syenogranite (SI/98/3 and SI/98/2A). They are subalkaline (Fig. 4A), moderately peraluminous (ASI between 1.1 and 1.2; Fig. 4B) and appear as highly differentiated granites (Fig. 4C). G_{2A} granites show REE patterns (Fig. 5E) typical for alkaline granites: high HREE (between 25 and 45 with SR6 at 130), low LREE/HREE fractionation (La_N/Yb_N between 4 and 18) and deep negative Eu anomaly (Eu/Eu^* between 0.24 and 0.49). Sample SR6 displays a seagull spectrum, typically resulting from late-magmatic fluids enriched in alkalies and associated elements such as fluorine. G_{2A} granite REE patterns are clearly above the reference $G_{1A–B}$ granite patterns (Fig. 5E). G_{2B} granites have patterns closer to those of $G_{1A–B}$ granites although with steeper HREE and deeper negative Eu anomalies (Fig. 5E). MORB-normalised spidergrams (Fig. 6E) confirm these observations: G_{2A} granite spectra, in addition to HREE,

are also richer in Hf and Zr and poorer in Sr than the $G_{1A–B}$ granites but are in the same range for Rb and Th, which is typical for alkaline series (Liégeois et al., 1998, and references therein). G_{2B} granites display their subalkaline character with lower abundance for most elements except for the most incompatible LILE elements (Th and Rb), which reflect their highly fractionated nature.

The two G_{2A} granites analysed for Nd isotopes point to strongly negative $\varepsilon_{Nd}(T)$ values of −8.8 to −10.0, with old T_{DM} Nd model ages of 2.85 and 3.23 Ga, indicating a major, if not total, contribution of the Archaean crust in their generation (Fig. 7).

5.6. G_4 magmatism

The large majority of the magmatic rocks in the Irumide Belt were emplaced during the Irumide Orogen (G_{4A}). These granitoids form large granite complexes engulfing all pre-existing lithologies in the southwestern Irumide Belt, including basement units of the Mkushi Gneiss ($G_{1A–B}$) and Lukamfwa ($G_{2A–B}$) suites, and overlying metasedimentary rocks of the Kanona/Manshya River Group (>1.88 Ga). In the northeastern Irumide Belt, G_4 granitoids also form discrete and well-delineated semi-circular plutons of batholithic (Bemba Batholith) or limited (singular bodies of the Chilubanama Granite) proportion. All G_4 granitoids are characterised by their coarse K-feldspar phenocrystic character, and granite types include coarse biotite granite, biotite-muscovite granite, biotite-hornblende granite and K-feldspar cumulate granite. Fabrics range from strongly foliated (augen) granite to undeformed coarse granite with primary magmatic layering defined by preferred orientation of K-feldspar phenocrysts parallel to the contacts with country rock. Chemically (Q′-ANOR classification of Streckeisen and Le Maître, 1979), they range from granodiorite to alkali-feldspar granite, most being monzogranite and syenogranite. One sample (ND5) has a lower content in quartz and corresponds to a quartz syenite. Twenty-one G_{4A} samples have been dated using the zircon U–Pb SHRIMP method, and they yielded crystallisation ages between 1053 ± 14 and 1005 ± 7 Ma (De Waele et al., 2003; De Waele, 2005). One G_{4B} alkali-feldspar granite (LW2) has been dated with the same method at 943 ± 5 Ma (De Waele, 2005).

The majority of the G_{4A} granitoids are subalkaline but a negligible number fall in the alkaline field (Fig. 4A). This is reflected by ASI values varying from 0.88 to 1.7 (0.6 for the ND4 hornblende granodiorite) although 80% of them have ASI values between 1.0 and 1.3. This is also displayed in Fig. 4C, where most G_{4A} granites are in the calc-alkaline field but where one-tenth of the samples fall in the alkaline field. The G_{4A} REE and trace element patterns (Figs. 5F and 6F) are variable: most lie within the $G_{1A–B}$ field but a series are above and are similar to the G_{2A} group, while some others mimic the G_{2B} group. It must be noted that, although representatives of these various kinds of G_{4A} granites have been dated within the 1050–1000 Ma range, no geochemical drift with time has been evidenced. G_{4B} granitoids are very low in LREE (La_N between 15 and 27 versus 38–460 for G_{4A}) and display low LREE:HREE fractionation (2.5–11 versus 4.3–83 for G_{4A}).

The two G_{4A} samples (ND4 and SR5) analysed for Nd isotopes show strongly negative initial $\varepsilon_{Nd}(T)$ value of −14.4 and −15.3 and Archaean T_{DM} Nd model ages of 3.32 and 2.64 Ga, indicating an overwhelming Archaean crustal component in their source.

5.7. The Sr isotopes: variably reset

Except for the basalts, poor in Rb, nearly all samples have Sr initial ratios (i.e. at zircon age) lower than 0.7 (Table 3), indicating later perturbation of the Rb–Sr isotopic system. The four G_{1C} Irumide rhyolites determine an isochron at 1160 ± 51 Ma (Sr initial ratio = 0.7213 ± 0.0018, MSWD = 1.04) and another with the same characteristic when adding the two Mansa G_{1C} granites: 1154 ± 50 Ma (Sr initial ratio = 0.7211 ± 0.0018, MSWD = 1.7).

This ca. 1150 Ma age broadly corresponds to classical ages on the Irumide Belt based on Rb–Sr and K–Ar methods (e.g. Fitches, 1968; Ray and Crow, 1975; Daly, 1986). Recent zircon age determinations however unequivocally show that the main Irumide event took place at 1.02 Ga (De Waele, 2005), indicating an important but only partial reset of the Rb–Sr isotopic system during the Irumide orogeny. The more mafic groups (G_{1C} basalts and G_{1C} dacites) plot below the isochron, which is related to their lower Rb content, while the $G_{1A–B}$ and G_2 granites plot close to the isochron. G_4 granites plot below the isochron, indicating their younger age. The data show that Sr isotopic ratios, unlike Nd isotopes, did not entirely keep a memory of the old source, and were significantly disturbed during the 1 Ga Irumide event. This can be directly linked to the much higher mobility of the alkaline and alkaline-earth elements and particularly to the higher mobility of Rb, as alkali diffusivities are orders of magnitude greater than non-alkali diffusivities (Baker, 1992). This means that the Sr isotopes cannot be used as geochronological or petrological tools in the Irumide region.

6. Discussion

6.1. A recurrent same Archaean crustal source over time

Except for the G_{1C} Katibunga basalts, all the Irumide and Mansa magmatic groups are felsic (65–78% SiO_2). All groups have Nd T_{DM} model ages significantly older than their zircon emplacement age. Moreover, these model ages are in the same age range, independently of the emplacement age (Fig. 7). A weighted average can be calculated at 2638 ± 130 Ma, which corresponds to the zircon age of the G_0 relic basement gneiss (2726 ± 36 Ma). A more detailed look shows:

(1) The older $G_{1A–B}$ groups (2.04–1.95 Ga) have T_{DM} older than 3 Ga (3.26 ± 0.23 and 3.13 ± 0.25 Ma), in agreement with a basement generated at 2.73 Ga in an Archaean continental arc, as suggested by the G_0 composition of TTG (Figs. 5A and 6A). The $G_{1A–B}$ groups can be considered as the result of the melting of a Neo-Archaean basement. The two known Archaean samples are probably not representative of this basement as they have La/Yb ratios which are too high to give a $G_{1A–B}$ melt. A full characterisation of the Archaean source material awaits additional data.
(2) The slightly younger G_{1C} group is represented by mafic and felsic volcanic rocks and high-level granitic plutons in both the Irumide and Mansa areas. As a mean, their T_{DM} model ages are younger than those of $G_{1A–B}$, ranging from 2.37 to 2.89 Ga (+KB9 at 3.16 Ga), and are not correlated: the weighted mean for the basalt is 2.64 ± 0.16 Ga (2.70 ± 0.29 with KB9) and 2.54 ± 0.15 Ga for the felsic rocks (granites, rhyolites and dacites). The Irumide rhyolites have a geochemical signature very close to the $G_{1A–B}$ groups, and a similar source and melting process can be envisaged for these G_{1C} lavas. Although slightly different, the geochemical and isotopic characteristics of the G_{1C} granites and dacites of the Bangweulu Block near Mansa indicate a similar Archaean cryptic basement below the Mansa area. The additional juvenile input needed to yield the observed Nd isotopic signature does not appear to translate into a significantly different geochemical composition for these felsic rocks. Generally, the basalts have lower spectra but the difference in abundance of the elements is roughly proportional to their incompatibility (Figs. 5C and 6C): similar for HREE, lower for LREE, K, Rb, Ba and Th. Three basalts of seven have, in addition, a negative anomaly in Zr–Hf. This suggests that these basalts could be able to produce the G_{1C} felsic rocks by differentiation or, more likely, that the, respectively, mafic and felsic sources of the G_{1C} basalts and G_{1C} felsic rocks were generated within a common petrogenetic process during the Archaean.
(3) The G_{2A} group appears to be alkaline, which agrees with the likely anorogenic character of this group, as no orogeny of this age (1.65–1.55 Ga) is known in Africa. The T_{DM} model ages are again in the same range as older suites (2.85 and 3.23 Ga). These characteristics can be reconciled by considering a lower degree of partial melting of the Archaean basement: only the more fusible part of the basement will melt and the incompatible elements will be enriched. With no knowledge on the composition of the Archaean basement and considering the variability of the partition coefficients for the felsic rocks, more detailed modelling based on available data is unlikely to yield better constraints.
(4) Only two Nd isotopic ratios are available for the voluminously dominant G_4 group. However, these are in the same range as the older groups (2.65 and 3.32 Ga), indicating that the G_4 group is again the result of the partial melting of the same Archaean crust. Its geochemistry spans the essentials of the $G_{1A–C}$ groups but also the alkaline G_2 group (Figs. 5 and 6), without any apparent age trend. This suggests that conditions prevailing for the generation of the G_1 and G_2 groups (i.e. varying degrees of partial melting) have alternated during the 50 million years (1050–1000 Ma) of the Irumide granite period.

It must be stressed that no other magmatic rock types are known in the Irumide and in the Mansa area leading to the conclusion that during the entire Proterozoic, the Irumide Belt was periodically the locus of crustal partial melting of its Archaean basement but with no addition of juvenile material, except in small amounts within the crustal melts themselves.

6.2. The Archaean Bangweulu Craton

The whole-rock geochemistry and isotopic constraints presented here indicate that the southern margin of the Bangweulu Block, and the Irumide Belt, are made up of a cryptic Archaean crust, remobilised several times during the Proterozoic. A similar scenario could be applied to the basement of the Domes region of the Copperbelt, where an Archaean basement has been evidenced on the basis of detrital zircons in the Muva Supergroup (peaks at 2.7 and at 3.02 and 3.2 Ga; Rainaud

et al., 2003) and more importantly, xenocrystic zircons of 3.2 Ga in volcanic units, and where granitoids at ca. 1.88 Ga are known (Ngoyi et al., 1991; John et al., 1999; Rainaud et al., 2002).

To the north of the Irumide Belt, the exposed part of the Bangweulu Block is made up of granitic basement, but the central part of the block is covered by sediments of the Muva Supergroup. The geodynamic evolution of the Bangweulu Block is considered to be entirely Proterozoic (Andersen and Unrug, 1984), but this was based only on Rb–Sr isochrons and K–Ar dates along the fringes of the block. At present no Nd isotopes or U–Pb zircon age data are available from the centre of the Bangweulu Block, but extrapolating from our data, we would suspect that such new data could reveal a covered Archaean source. As the Palaeoproterozoic sediments (Muva Supergroup) are nearly undeformed platform sediments which have escaped Mesoproterozoic deformations of the Irumide Orogen, and rest on a cratonic area (Daly and Unrug, 1982), no late Mesoproterozoic magmatism would be expected there. These observations and our data suggest that the Bangweulu Block, when considering its entire lithosphere, is an Archaean Craton, solving the so-called Bangweulu paradox, i.e. the fact that the Bangweulu Block was sutured to the Tanzania Craton along a collisional belt which appears to predate the dated undeformed magmatic units of the Bangweulu Block by 200 million years.

6.3. The metacratonic evolution of the Bangweulu Craton during Irumide tectonism

The Irumide Belt is characterised by the coexistence of preserved Palaeoproterozoic basement and supracrustal successions with shallow-level late Mesoproterozoic granitoid plutons, and upper amphibolite grade gneisses indicating pressures of up to 8 kbar and temperatures of 650 °C (De Waele et al., 2005). These lateral associations strongly support dominant vertical block-tectonics, the recorded crustal shortening within the supracrustals and basement gneisses recorded by Daly (1986) pointing to a thin-skin thrust tectonic style. The supracrustal succession (the Muva Supergroup) displays a gradient from unmetamorphosed to upper amphibolite metamorphic facies from north to south (Daly and Unrug, 1982). All these observations allow one to consider the Irumide Belt as the partly reworked southern margin of the Bangweulu Block. The rock assemblages, geochemical nature and isotopic constraints of the granitoids and the volcanic rocks indicate that only insignificant amounts of juvenile material were added within the southern Bangweulu Block margin during the entire Proterozoic. This strongly suggests that this region was never an active margin during the Palaeo- and Mesoproterozoic but was in the position of a passive margin. Passive margins, even if cratonic, can be affected by intercontinental collision, leading to the concept of a metacraton (Abdelsalam et al., 2002; Liégeois et al., 2003). A passive margin occurs on an advancing plate that is being subducted beneath an opposing active margin. During collision, the continental part of this plate may begin to subduct and is therefore subjected to higher pressure, temperature and stress until the collision stops and the orogen is subjected to uplift. However, due to the thick lithosphere of a craton (e.g. Black and Liégeois, 1993, and references therein), this reactivation is not total and is concentrated along pre-existing shear zones and marked by high-temperature metamorphism and crustal granitoids (Liégeois et al., 2003).

Such a model implies that the studied region, i.e. the Irumide Belt, is located close to the suture zone with the other continent (the former active margin). We suggest that the active margin may be represented by the Southern Irumide Belt to the south of the Karoo grabens. The Southern Irumide Belt consists of late Mesoproterozoic, broadly contemporaneous juvenile terranes (Oliver et al., 1998; Johnson, 1999; Johnson and Oliver, 2000, 2004; Johnson et al., 2005a,b). We also suggest that the Karoo graben in between the Irumide and Southern Irumide Belts may reuse a lithospheric discontinuity that could represent a late Mesoproterozoic suture. This would imply a former palaeo-Benioff plane with a slope below the Southern Irumide Belt, directed towards the SE. It must be stressed that such lithospheric boundaries are often the locus of post-collisional transpression (Liégeois et al., 1998, 2003), suggesting that horizontal movements were likely occurring between the Irumide and the Southern Irumide at ca. 1 Ga. Such post-collisional transcurrent movements could explain the diachronism existing between the Irumide and Southern Irumide Belt.

In contrast, such horizontal movements were probably limited inside the former cratonic passive margin constituted by the Irumide Belt, i.e. in the metacratonic margin of the Bangweulu Craton. The latter was mainly affected by differential vertical movements when the subducted continental plate popped up at the end of the collision (i.e. the initial impact following the nomenclature of Liégeois et al., 1998), initiating the post-collisional period. Such limited lateral tectonic movements inside the Irumide Belt agree with the isotopic and geochemical data indicating that the same source was melted several times during the Proterozoic. The apparent homogeneity of the Archaean source was fur-

ther amplified by renewed crustal melting during the successive thermal episodes, leading to homogenisation and the production of magmas similar in composition to eutectic melt. The lack of a mantle-contribution (juvenile component) in the magmatic suites of the region signifies that the mantle-derived magma produced below the former active margin was not able to pass through the Irumide lithosphere, but managed to heat up sections of the Irumide lower crust sufficiently to invoke large-scale reworking in the upper crust.

6.4. The Bangweulu metacraton and its relation with neighbouring cratons

Prior to the metacratonisation of the Bangweulu Craton during Irumide orogenesis, the region appears to have been subjected to several older events leading to magmatic units of strikingly similar character to G_4 magmatism. The main older event was the G_1 event, which, as with G_4 magmatism, produced no juvenile material. It comprises only crustal granitoids and volcanics, and shows no evidence for an active margin. Unlike the G_4 event however, these magmatic episodes ($G_{1A–C}$) seem to have affected the entire exposed part of the Bangweulu Block and the adjacent Ubendian Belt. As a working hypothesis, we suggest that the Bangweulu Block could represent a wide metacratonic boundary of a larger craton, from which it may subsequently have been detached. A similar scenario has been suggested for the LATEA metacraton in Hoggar (Liégeois et al., 2003). Should this be the case, the question remains of whether the Bangweulu Block formed part of the Tanzania Craton to the east, implying limited or only transverse movements along the Ubendian Belt, or of the Kasai/Congo Craton to the north, implying limited movements along the Kibaran Belt at ca. 1.38 Ga. It is worth noting that the Muva sedimentary successions thicken from the centre of the Bangweulu Block towards the Irumide Belt, while G_{1C} magmatism appears to be of a higher level character on the Bangweulu Block than in the Irumide Belt. Moreover, G_{1C} granitoids and volcanic units occur over a distance of at least 1000 km from the Usagaran Belt in the east to the Domes region of the Copperbelt in the west, arguing in favour of a north–south oriented convergence during the Palaeoproterozoic.

6.5. The Lukamfwa episode

The Lukamfwa episode at 1.66–1.55 Ga represents a low-volume event, at a period when there was no (documented) orogeny in Africa and, compared to the other Irumide magmatic groups, was more alkaline in nature. However, its Nd T_{DM} model ages are similar to the G_1 group, suggesting that the same crustal source was tapped, but with a lower degree of partial melting of the more fusible parts of the underlying Archaean crust. $G_{2A–B}$ magmatism was only located within the Irumide Belt, the most metacratonic part of the Bangweulu Block, suggesting that the generation of the group could have been triggered by reactivation of metacratonic faults or shear zones due to far-field stresses, as proposed for the Pan-African LATEA metacraton in Hoggar for the Cambrian Taourirt high-level plutons (Azzouni-Sekkal et al., 2003) and for the Cenozoic volcanism (Liégeois et al., 2005). It is difficult to speculate on the exact nature of the tectonic processes responsible for these far-field stresses. On the African continent, no convergent tectonic processes have been documented that could account for reactivation along the Irumide margin meaning that a matching orogenic episode must be sought outside the African continent.

7. Conclusions

The Irumide Belt appears to be the metacratonic boundary of the Bangweulu Block. Such a structure can result from the effects of convergence on the trailing part of the continent (passive margin). During the collision, this continental fragment, devoid of any subduction-related magmatism, is briefly but potentially deeply subducted. Eventually, this process leads to cessation of subduction, but during this short but major process, the cratonic passive margin is submitted to high pressure, temperature and stress. This can lead to reactivation of pre-existing lithospheric shear zones and the generation of high temperature metamorphism and crustal melting giving rise to large quantities of granitoids and felsic volcanic rocks. Such metacratonic areas are often bound by mega-shear zones corresponding to sutures with, on the other side, more juvenile terranes corresponding to the former active margin of the collider. Because of the rigid, but strongly dissected nature of metacratonic boundaries, they are often the locus of recurrent major horizontal movements along prominent lithospheric structures.

During the Proterozoic, the Irumide Belt has been the locus of two main metacratonic evolutions (Usagaran phase, ca. 2.03 Ga and Irumide phase at ca. 1.02 Ga) and of several major reactivations (late Usagaran phase, ca. 1.94, Ubendian phase, ca. 1.87 and Lukamfwa phase, ca. 1.6 Ga) affecting an Archaean craton. A succession of proposed tectonic events and their timing are shown in Fig. 8 and a simplified tectonic map showing the various tectonic units and the extent of the Bangweulu Metacraton is shown in Fig. 9.

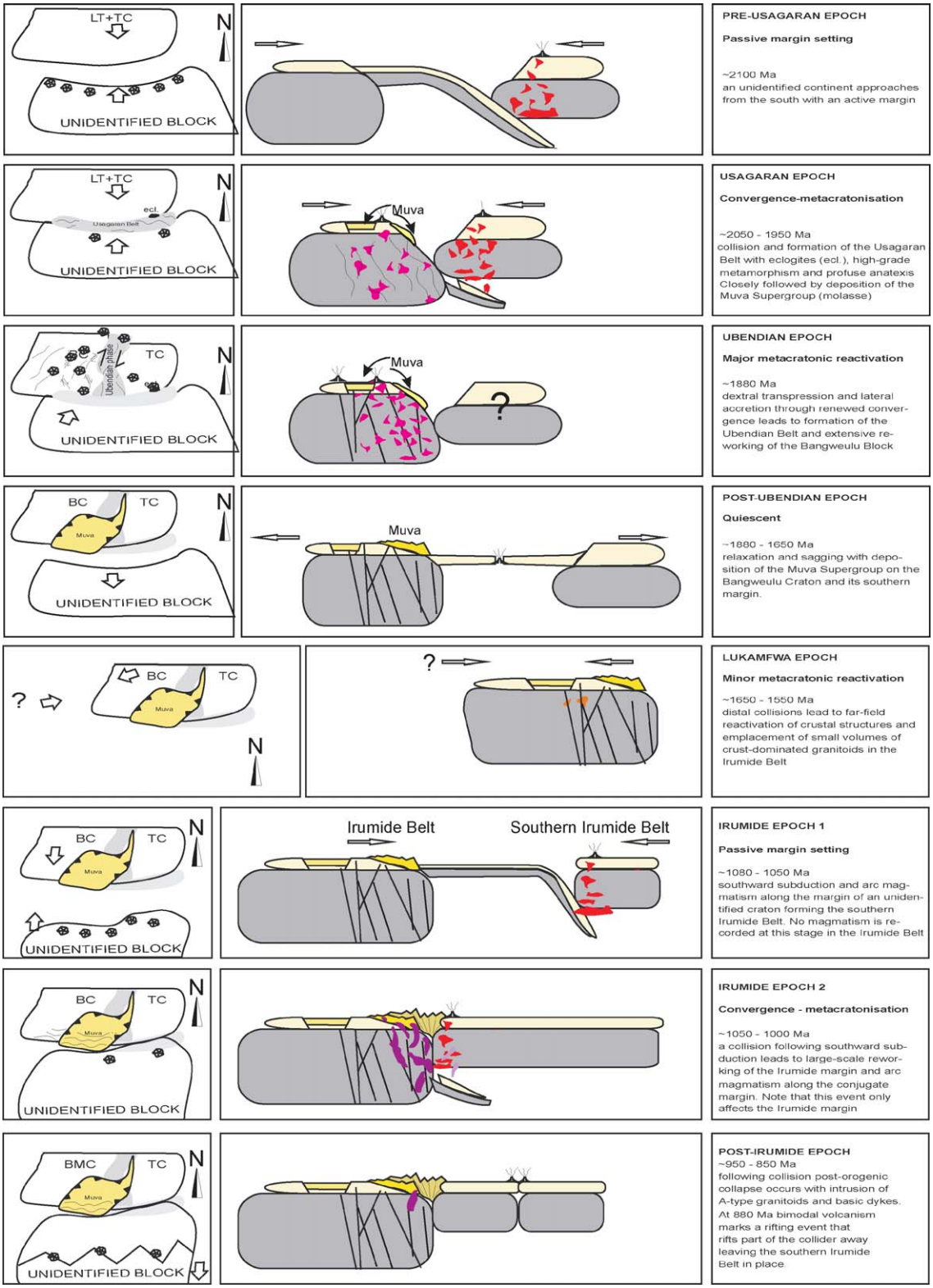

Fig. 8. Simplified cartoon of the tectonic development of the Bangweulu metacraton and the Irumide Belt. Left: simplified plan views; middle: schematic cross-section view; right: brief description of tectonic event(s).

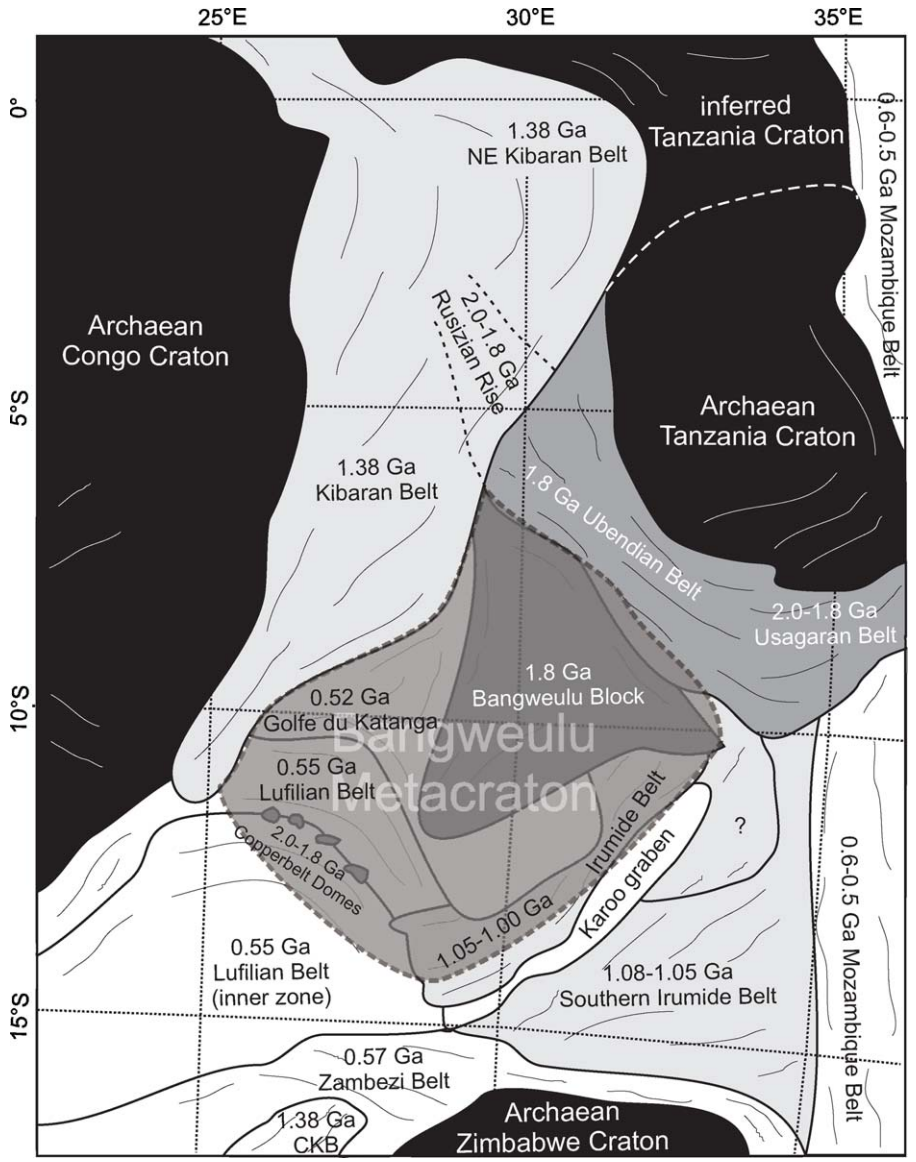

Fig. 9. Schematic tectonic map showing the proposed extent of Archaean cratons and the Bangweulu metacraton.

These metacratonic events generated: (1) mainly vertical movements along pre-existing structures, juxtaposing contemporaneous metamorphic and unmetamorphosed lithologies; (2) granitoids and volcanic rocks resulting from the partial melting of the cratonic Bangweulu Archaean lower crust sharing the same Archaean (ca. 3 Ga) Nd T_{DM} model ages and global geochemistry whatever their emplacement ages over more than 1 billion years.

The Irumide Belt was successively intruded by the Ubendian G_{1A} (2.04–2.03 Ga) and G_{1B} (1.95–1.93 Ga) groups, the Usagaran G_{1C} (1.88–1.85 Ga) group, coeval with passive margin sedimentation (the Muva Supergroup), the Lukamfwa $G_{2A–B}$ (1.66–1.61 Ga) group, more alkaline due to a lower degree of partial melting of the old crust, and finally by the G_4 group during the time of Rodinia assembly at 1.02 billion years ago. This last event led to the dominant structural features preserved in the Irumide Belt, largely obliterating previous structural records, but because of the metacratonic character of the Irumide Belt, allowed the preservation of older lithologies such as the ca. 1.87 Ga Katibunga basalts and the subcontemporaneous Muva Supergroup. No active margin related rocks are known in the Irumide Belt, but juvenile Irumide-aged terranes are known in the Southern Irumide Belt, just south of the MDZ (now marked by a

Karoo graben) marking the southern limit of the Irumide Belt. The slightly older ages of the Southern Irumide terranes (1.08–1.04 Ga) are consistent with their generation prior to final collision of two continents fragments.

Whereas metacratonisation during the 1 Ga Irumide Orogeny affected only the southern part of the Bangweulu Block, tectonism at ca. 2 Ga appears to have been more widespread and affected the entire Bangweulu Block. This suggests that the Bangweulu Block itself was actually the metacratonic boundary of a larger Archaean craton, either the Tanzania Craton or an Archaean part of the Congo Craton.

Acknowledgements

This is Tectonics Special Research Centre publication number 362. The authors would like to thank the reviewers and editor for valuable comments and suggestions which have helped improve the manuscript. We would like to extend our gratitude to the staff at the Department of Applied Chemistry at Curtin University of Technology for assistance with the geochemical analyses. Much of the work in the field was made possible through the help of the Department of Geology at the University of Zambia. This paper is dedicated to the late Prof. A.B. Kampunzu and Dr. Crispin Katongo.

References

Abdelsalam, M.G., Liégeois, J.-P., Stern, R.J., 2002. The Saharan Metacraton. J. Afr. Earth Sci. 34, 119–136.

Ackermann, E.H., 1950. Ein neuer faltengurtel in Nordrhodesien und seine tectonische stellung im Afrikanishen grundgebirge. Geologische Rundsch. 38, 24–39.

Andersen, L.S., Unrug, R., 1984. Geodynamic evolution of the Bangweulu block, northern Zambia. Precambrian Res. 25, 187–212.

Andrews-Speed, C.P., 1986. Gold-bearing fluvial and associated tidal marine sediments of Proterozoic age in the Mporokoso basin, northern Zambia. Sedimentary Geol. 48, 193–222.

Andrews-Speed, C.P., 1989. The Mid-Proterozoic Mporokoso basin, northern Zambia: sequence stratigraphy, tectonic setting and potential for gold and uranium mineralisation. Precambrian Res. 44, 1–17.

Azzouni-Sekkal, A., Liégeois, J.-P., Bechiri-Benmerzoug, F., Belaidi-Zinet, S., Bonin, B., 2003. The "Taourirt" magmatic province, a marker of the very end of the Pan-African orogeny in the Tuareg Shield: review of available data and Sr–Nd isotope evidence. J. Afr. Earth Sci. 37, 331–350.

Baker, D.R., 1992. Estimation of diffusion coefficients during interdiffusion of geologic melts: application of transition state theory. Chem. Geol. 98, 11–21.

Black, R., Liégeois, J.P., 1993. Cratons, mobile belts, alkaline rocks and continental lithospheric mantle; the Pan-African testimony. J. Geol. Soc. Lond. 150 (1), 89–98.

Brewer, M.S., Haslam, H.W., Darbyshire, P.F.P., Davis, A.E., 1979. Rb–Sr Age Determinations in the Bangweulu Block, Luapula Province, Zambia, vol. 79/5. Institute of Geological Sciences, London.

Bulambo, M., De Waele, B., Kampunzu, A.B., Tembo, F., 2004. SHRIMP U-Pb geochronology of the Choma-Kalomo block (Zambia) and geological implications, 20th Colloquium of African Geology, Orléans, France, p. 96.

Cahen, L., et al., 1984. The Geochronology and Evolution of Africa. Oxford University Press, Oxford, 512 pp.

Clarke, D.B., 1992. Granitoid Rocks. Chapman & Hall, London, 283 pp.

Clifford, T.N., 1970. The structural framework of Africa. In: Clifford, T.N., Gass, I.G. (Eds.), African Magmatism and Tectonics. Oliver and Boyd, Edinburgh, pp. 1–26.

Cox, K.G., Bell, J.D., Pankhurst, R.J., 1979. The Interpretation of Igneous Rocks. George Allen & Unwin, London, 445 pp.

Cox, R.A., Rivers, T., Mapani, B., Tembo, D., De Waele, B., 2002. New U-Pb data for the Irumide belt: LAM-ICP-MS results for Luangwa Terrane. In: Namibia, G.S.O. (Ed.), 11th IAGOD Quadrennial Symposium and Geocongress, Technical Meeting IGCP 440: Assembly and Breakup of Rodinia. Windhoek, Namibia, p. 10.

Crock, J.G., Lichte, F.E., 1982. Determination of rare earth elements in geologic materials by inductively couple argon plasma/atomic emission spectrometry. Anal. Chem. 54, 1329–1332.

Daly, M.C., 1986. The tectonic and thermal evolution of the Irumide belt, Zambia. Ph.D. Thesis. University of Leeds, Leeds, 326 pp.

Daly, M.C., 1988. Crustal shear zones in central Africa. A kinematic approach to Proterozoic tectonics. Episodes 11, 5–11.

Daly, M.C., 1995a. The Geology of Chinsali and Mutangoshi Hills Area; Explanation of Degree Sheet 1032, SE and SW Quarter, vol. 79. Geological Survey Department of Zambia, Lusaka.

Daly, M.C., 1995b. The Geology of Mulilansolo Mission and Isoka Areas; Explanation of Degree Sheet 1032, NE and NW Quarter, vol. 84. Geological Survey Department of Zambia, Lusaka.

Daly, M.C., Unrug, R., 1982. The Muva Supergroup, northern Zambia. Trans. Geol. Soc. S. Af. 85, 155–165.

De Waele, B., 2005. The Proterozoic geological history of the Irumide belt, Zambia. Ph.D. Thesis. Curtin University of Technology, Perth, 468 pp.

De Waele, B., Fitzsimons, I.C.W., 2004. The Age and Detrital Fingerprint of the Muva Supergroup of Zambia: Molassic Deposition to the Southwest of the Ubendian Belt. Geoscience Africa, Johannesburg, South Africa, pp. 162–163.

De Waele, B., Johnson, S.P., Fitzsimons, I.C.W., Wingate, M.T.D., Mapani, B.S.E., Tembo, F., 2005. Does the record of punctuated magmatism and late Mesoproterozoic tectonism along the southern margin of the Congo Craton support a continent-spanning "Kibaran" event during the formation of Rodinia? Gondwana-12: "Geological and Biological heritage of Gondwana", Mendoza, Argentina.

De Waele, B., Mapani, B., 2002. Geology and correlation of the central Irumide belt. J. Afr. Earth Sci. 35 (3), 385–397.

De Waele, B., Wingate, M.T.D., Mapani, B., Fitzsimons, I.C.W., 2003. Untying the Kibaran knot: a reassessment of Mesoproterozoic correlations in southern Africa based on SHRIMP U–Pb data from the Irumide belt. Geology 31 (6), 509–512.

De Waele, B., Kampunzu, A.B., Mapani, B.S.E., Tembo, F., in press. The Irumide Belt of Zambia. J. Afr. Earth Sci.

Dodson, M.H., Cavanagh, B.J., Thatcher, E.C., Aftalion, M., 1975. Age limits for the Ubendian metamorphic episode in northern Malawi. Geol. Mag. 112, 403–410.

Drysdall, A.R., Johnson, R.L., Moore, T.A., Thieme, J.G., 1972. Outline of the geology of Zambia. Geologie en Mijnbouw 51, 265–276.

Fitches, W.R., 1968. New K–Ar Age Determinations from the Pre-Cambrian Mafingi Hills Area of Zambia and Malawi, vol. 12. Research Institute for African Geology, Leeds.

Gromet, L.P., Dymek, R.F., Haskin, L.A., Korotev, R.L., 1984. The "North American shale composite"; its compilation, major and trace element characteristics. Geochim. Cosmochim. Acta 48 (12), 2469–2482.

Hanson, R.E., Wilson, T.J., Wardlaw, M.S., 1988a. Deformed batholiths in the Pan African Zambezi belt, Zambia: age and implications for regional Proterozoic tectonics. Geology 16, 1134–1137.

Hanson, R.E., Wilson, T.J., Brueckner, H.K., Onstott, T.C., Wardlaw, M.S., Johns, C.C., Hardcastle, K.C., 1988b. Reconnaissance geochronology, tectonothermal evolution, and regional significance of the Middle Proterozoic Choma-Kalomo block, southern Zambia. Precambrian Res. 42, 39–61.

Hunter, D.R., 1981. Precambrian of the Southern Hemisphere. Elsevier, Amsterdam.

Irvine, T.N., Baragar, W.R.A., 1971. A guide to the chemical classification of the common volcanic rocks. Can. J. Earth Sci. 8, 523–548.

John, T., 2001. Subduction and continental collision in the Lufilian Arc–Zambezi belt orogen: a petrological, geochemical, and geochronological study of eclogites and whiteschists (Zambia). Ph.D. Thesis. University of Kiel, Kiel, 78 pp.

John, T., Schenk, V., Tembo, F., 1999. The metamorphic evolution and U/Pb dating of monazites of the southern Irumide Belt, SE-Zambia. In: De Waele, B., Tembo, F., Key, R.M. (Eds.), Abstracts Volume IGCP 419/419. Geological Society of Zambia, Lusaka, p. 7.

Johnson, S., 1999. A Kibaran aged marginal basin and island-arc complex in northern Zimbabwe. In: De Waele, B., Tembo, F., Key, R.M. (Eds.), Abstracts Volume IGCP 418/419. Geological Society of Zambia, Lusaka, p. 6.

Johnson, S.P., De Waele, B., Tani, K., Tembo, F., 2005a. Mesoproterozoic supra-subduction magmatism in the southern Irumide Belt, central southern Africa: implications for the Congo Craton in Rodinia reconstructions. In: Supercontinents and Earth Evolution Symposium, Fremantle, Western Australia.

Johnson, S.P., Rivers, T., De Waele, B., 2005b. A review of the Mesoproterozoic to early Palaeozoic magmatic and tectonothermal history of south-central Africa: implications for Rodinia and Gondwana. J. Geol. Soc. Lond. 162, 433–450.

Johnson, S.P., Oliver, G.J.H., 2000. Mesoproterozoic oceanic subduction, island-arc formation and the initiation of back-arc spreading in the Kibaran belt of central, southern Africa: evidence from the ophiolite terrane, Chewore inliers, northern Zimbabwe. Precambrian Res. 103, 125–146.

Johnson, S.P., Oliver, G.J.H., 2004. Tectonothermal history of the Kaourera Arc, northern Zimbabwe: implications for the tectonic evolution of the Irumide and Zambezi Belts of south central Africa. Precambrian Res. 130, 71–97.

Kabengele, M., Lubala, R.T., Cabanis, B., 1991. Caractérisation pétrologiques et géochimique du magmatisme ubendien du secteur de Pepa-Lubumba, sur le plateau des Marungu (Nord-Est du Shaba, Zaire). Signification géodynamique dans l'évolution de la chaine ubendienne. J. Afr. Earth Sci. 13 (2), 243–265.

Katongo, C., et al., 2004. Petrography, geochemistry and geochronology of granitoid rocks in the Neoproterozoic-Paleozoic Lufilian – Zambezi belt, Zambia: implications for tectonic setting and regional correlation. J. Afr. Earth Sci. 40, 219–244.

Key, R.M., Liyungu, A.K., Njamu, F.M., Somwe, V., Banda, J., Mosley, P.N., Armstrong, R.A., 2001. The western arm of the Lufilian Arc in NW Zambia and its potential for copper mineralisation. J. Afr. Earth Sci. 33, 503–528.

Kleinhanns, I.C., Kramers, J.D., Kamber, B.S., 2003. Importance of water for Archaean granitoid petrology: a comparative study of TTG and potassic granitoids from Barberton Mountain Land, South Africa. Contrib. Mineral. Petrol. 145 (3), 377–389.

Klerkx, J., Theunissen, K., Delvaux, D., 1998. Persistent fault controlled basin formation since the Proterozoic along the Western Branch of the East African Rift. J. Afr. Earth Sci. 26 (3 SU), 347–361.

Kröner, A., 1977. The Precambrian geotectonic evolution of Africa: plate accretion versus plate destruction. Precambrian Res. 4, 163–213.

Kuno, H., 1966. Lateral variation of basalt magma type across continental margins and island arcs. Bull. Volcanol. 29, 195–222.

Lenoir, J.L., Liégeois, J.-P., Theunissen, K., Klerkx, J., 1994. The Palaeoproterozoic Ubendian shear belt in Tanzania: geochronology and structure. J. Afr. Earth Sci. 19 (3), 169–184.

Liégeois, J.-P., Benhallou, A., Azzouni-Sekkal, A., Yahiaoui, R., Bonin, B., 2005. The Hoggar swell and volcanism: reactivation of the Precambrian Tuareg shield during Alpine convergence and West African Cenozoic volcanism. In: Foulger, G.R., Natland, J.H., Presnall, D.C., Anderson, D.L. (Eds.), Plates, Plumes and Paradigms. Geological Society of America, pp. 379–400.

Liégeois, J.-P., Navez, J., Hertogen, J., Black, R., 1998. Contrasting origin of post-collisional high-K calc-alkaline and shoshonitic versus peralkaline granitoids. The use of sliding normalization. Lithos 45, 1–28.

Liégeois, J.P., Latouche, L., Boughrara, M., Navez, J., Guiraud, M., 2003. The LATEA metacraton (Central Hoggar, Tuareg shiled, Algeria): behaviour of an old passive margin during the Pan-African orogeny. J. Afr. Earth Sci. 37, 161–190.

Lugmair, G.W., Marti, K., 1978. Lunar initial $^{143}Nd/^{144}Nd$; differential evolution of the lunar crust and mantle. Earth Planet. Sci. Lett. 39 (3), 349–357.

Maniar, P.D., Piccoli, P.M., 1989. Tectonic discrimination of granitoids. Geol. Soc. Am. Bull. 101, 635–643.

Nelson, B.K., DePaolo, D.J., 1985. Rapid production of continental crust 1.7–1.9 b.y. ago: Nd and Sr isotopic evidence from the basement of the North American midcontinent. Bull. Geol. Soc. Am. 96, 746–754.

Ngoyi, K., Liégeois, J.-P., Demaiffe, D., Dumont, P., 1991. Age tardi-ubendien (Protérozoïque inférieur) des dômes granitiques de l'arc cuprifére zaïro-zambien. C.R. Acad. Sci. 313 (II), 83–89.

Oliver, G.J.H., Johnson, S.P., Williams, I.S., Herd, D.A., 1998. Relict 1.4 Ga oceanic crust in the Zambezi Valley, northern Zimbabwe: evidence for Mesoproterozoic supercontinental fragmentation. Geology 26, 571–573.

Rainaud, C., Master, S., Armstrong, R.A., Robb, L.J., 2005. Geochronology and nature of the Palaeoproterozoic basement in the Central African Copperbelt (Zambia and the Democratic Republic of Congo), with regional implications. J. Afr. Earth Sci. 42, 1–31.

Rainaud, C., Master, S., Armstrong, R.A., Robb, L.J., 2003. A cryptic Mesoarchean terrane in the basement to the central African Copperbelt. J. Geol. Soc. Lond. 160, 11–14.

Rainaud, C.L., Armstrong, R.A., Master, S., Robb, L.J., Mumba, P.A.C.C., 2002. Contributions to the geology and mineralisation of the central African Copperbelt: I. Nature and geochronology of the pre-Katangan basement. In: Namibia, G.S.O. (Ed.), 11th IAGOD Quadrennial Symposium and Geocongress. Geological Survey of Namibia. Windhoek, Namibia, p. 5.

Ray, G.E., Crow, M.J., 1975. A review of some age determinations from the Misuku belt of northern Malawi. Rec. Geol. Surv. Malawi 8, 49–66.

Ring, U., Kröner, A., Layer, P., Buchwaldt, R., Toulkeredis, T., 1999. Deformed A-type granites in northern Malawi, east-central Africa: pre- or syntectonic. J. Geol. Soc. Lond. 156, 695–714.

Ring, U., Kröner, A., Toulkeredis, T., 1997. Palaeoproterozoic granulite-facies metamorphism and granitoid intrusions in the Ubendian-Usagaran Orogen of northern Malawi, east-central Africa. Precambrian Res. 85, 27–51.

Schandelmeier, H., 1980. Regionale gliederung des Prakambriums und aspekte der krustentwicklung um Mambwe/nordost-Zambia. Ph.D. Thesis. Technical University of Berlin, Berlin, 134 pp.

Schandelmeier, H., 1983. The geochronology of post-Ubendian granitoids and dolerites from the Mambwe area, northern province, Zambia. Rep. Inst. Geol. Sci. 83 (1), 40–46.

Schenk, V., Appel, P., 2001. Anti-clockwise P-T path during ultrahigh-temperature (UHT) metamorphism at ca. 1050 Ma in the Irumide Belt of Eastern Zambia. Berichte der Deutschen Mineralogischen Gesellschaft. Beihefte zum Eur. J. Mineral. 13, 161.

Steiger, R.H., Jäger, E., 1977. Subcommission on geochronology: convention on the use of decay constants in geo- and cosmochronology. Earth Planet. Sci. Lett. 36, 359–362.

Streckeisen, A., Le Maître, R.W., 1979. A chemical approximation to the modal QAPF classification of the igneous rocks. Neues Jahrbuch fuer Mineralogie. Abhandlungen 136 (2), 169–206.

Sun, S.-S., 1982. Chemical composition and origin of the Earth's primitive mantle. Geochem. Cosmochem. Acta 179–192, 46.

Sylvester, P.I., 1989. Post-collisional alkaline granites. J. Geol. 97, 261–280.

Taylor, S.R., McLennan, S.M., 1985. The Continental Crust: Its Composition and Evolution. Blackwell Scientific Publications, Oxford, 312 pp.

Tembo, F., 1986. Petrology and geochemistry of syenite intrusions in the eastern province of Zambia. M.Sc. Thesis. University of Zambia, Lusaka.

Tembo, F., De Waele, B., Nkemba, S., 2002. Syn- to post-orogenic granitoid magmatism in the Irumide Belt of Zambia: geochemical evidence. Afr. Geol. Rev. 9 (1), 1–17.

Unrug, R., 1984. The Mid-Proterozoic Mporokoso Group of northern Zambia: stratigraphy, sedimentation and regional position. Precambrian Res. 24, 99–121.

Vrána, S., Kachlík, V., Kröner, A., Marheine, D., Seifert, A.V., Îáãek, V., BabÛrek, J., 2004. Ubendian basement and its late Mesoproterozoic and early Neoproterozoic structural and metamorphic overprint in northeastern Zambia. J. Afr. Earth Sci. 38, 1–21.

Winter, J., 2001. An Introduction to Igneous and Metamorphic Petrology. Prentice Hall, 697 pp.